ATLAS PUB Note

ATL-PHYS-PUB-2021-034

30th July 2021

Towards a precise interpretation of the top quark mass parameter in ATLAS Monte Carlo samples

The ATLAS Collaboration [1]

This note relates the top quark mass parameter in simulated pp collisions with a 13 TeV centre-of-mass-energy produced by ATLAS to a well-defined field-theoretical mass scheme. A calibration for the top mass parameter in simulation is obtained by fitting the simulated jet mass distribution of large–radius jets containing hadronically-decaying top quark with large transverse momentum, with a particle-level calculation at next-to-leading-log precision. The relation between the top mass parameter in the nominal Powheg + Pythia 8 simulation and the MSR mass scheme is determined to be:

$$\Delta^{MSR} = m_t^{\mathrm{MC}} - m_t^{\mathrm{MSR}}(1\ \mathrm{GeV}) = 80^{+350}_{-400}\ \mathrm{MeV},$$

where the uncertainty is dominated by contributions from uncalculated higher orders in the NLL calculation, the fit methodology and underlying event modelling.

[1] The full author list can be found at:
https://atlaspo-eos.web.cern.ch/authorlists/PUB-TOPQ-2020-18/atlas_authlist.pdf.

Contents

1 Introduction

The existence of all particles predicted by the Standard Model (SM) has been verified experimentally following the discovery of the Higgs boson in 2012 by the ATLAS [1, 2] and CMS [3, 4] collaborations at CERN's Large Hadron Collider (LHC) [5]. The Higgs boson endows other fundamental particles with mass, and couples most strongly to the top quark. The strength of this coupling, and the resulting large value of the top quark mass, implies that precise measurements of the top mass are powerful constraints of the electroweak sector of the SM [6, 7].

Measurements of the top quark mass have been a central component of experimental programmes at both the the Tevatron and LHC since the particle's discovery [8, 9]. Recent 'direct' mass measurements at the LHC experiments have reached a precision of approximately 500–600 MeV [10–12], and the Tevatron average has a similar precision [13]. These measurements are generally in agreement with each-other and the precision can be improved further by combining measurements in different experiments and in different final states [14]. Direct measurements utilise templates derived from Monte Carlo (MC) simulated events with different values of the generator top mass parameter, m_t^{MC}, and a detailed simulation of the experimental detector response. Measurements following this approach in non-standard final states [15], in single-top production [16–18] and in high-p_{T} top-quark production [19] yield compatible results, with levels of precision typically around 1.2 – 2.5 GeV.

In quantum field theory, the notion of the mass of a fundamental particle like the top quark corresponds to defining a parameter in the underlying Lagrangian. Due to the presence of radiative corrections there is no unique definition for the renormalized mass parameters, and different choices are referred to as mass schemes. The best-fit value of the MC mass parameter, m_t^{MC}, is usually identified with the top-quark mass in the pole scheme, m_t^{pole}. This interpretation is correct within a precision of ~0.5 GeV [20]. Further discussions of the interpretation of the top quark mass measurements are found in Section 6.5.1 of the HL-LHC Yellow Report [21] and in Refs. [22, 23].

Perturbative and non-perturbative quantum chromodynamics (QCD) effects of this order are uncontrolled in the Monte Carlo generators and can affect the meaning of the top mass parameter. A well-understood example of such an effect is the infrared cut-off Q_0 in the angle–ordered Herwig parton shower [24, 25], which has been shown to cause a sizeable perturbative correction between m_t^{MC} and m_t^{pole} [26]. The choice of colour reconnection, fragmentation model and recoil schemes can also affect the relationship between the MC top mass and physics observables, at a similar level [27–30]. Furthermore, the top quark pole mass contains an infrared renormalon abiguity which amounts to 110-250 MeV at asymptotic higher order [31, 32]. Therefore, the pole mass value depends strongly on the order in NLO and NNLO fixed-order calculation. This order-dependence can exceed 250 MeV. In practice, these ambiguities in the definition of the top quark mass are often assigned as an additional uncertainty of 0.5 GeV, for instance in precision fits of the SM electroweak sector [33]. This additional uncertainty limits the potential impact of top mass measurements when checking the internal consistency of the SM.

Another category of top-quark mass measurements have been developed which do not depend on templates derived from Monte Carlo simulation. Such 'indirect' measurements extract m_t^{pole} from measurements of observables such as the inclusive top-quark pair-production cross section using fixed-order calculations at parton-level. This approach offers more flexibility to choose the mass scheme [34], but the precision is currently limited around $\sim$ 2 GeV due to the relatively poor sensitivity of the total cross-section to m_t^{pole} when compared to direct measurements. More precise determinations are possible from differential cross section measurements [35–37].

This note is the first step in a series of studies which aim to clarify the interpretation of m_t^{MC} by deriving a relation between the top mass parameter in event generators and a well-defined mass scheme using an analytic calculation in perturbative QCD. The Monte Carlo generators developed by the HEP community over the course of several decades provide a very good description of a broad range of differential cross sections. However, the formal accuracy for MC description of observables sensitive to soft and collinear QCD effects described by parton shower is only leading logarithmic for most observables, that is often made up for via tuning the hadronization model. There are also limitations concerning the treatment of finite lifetime effects, where MC generators typically use the Narrow Width Approximation [2]. This approximation particularly impacts the top quark mass determinations, where the uncertainties are already much smaller than the top quark width. By comparing the MC prediction at particle-level to more accurate first-principle calculations, with systematic field theoretic treatment of perturbative and non-perturbative (hadronization) effects as well as finite lifetime effects, a more rigorous extraction of the SM Lagrangian parameters can be performed. This is the motivation of the calibration procedure carried out in this note.

The technique described here is based on the proposal in Ref. [40]. The e^+e^- calculation used there was extended to NNLO+NNNLL precision in Ref. [41] and to hadron collider observables at NLL precision in Ref. [42]. Here, the procedure is applied to simulated $t\bar{t}$ samples produced by ATLAS for use in top

[2] The narrow width approximation can be avoided for certain final states using the Powheg $b\bar{b}4l$ model of Ref. [38, 39], but to-date, top quark measurements are based on the hvq model.

physics analysis during Run 2. A relation between m_t^{MC} and a top mass defined in a field-theoretical mass scheme is obtained by fitting NLL predictions to the jet mass distribution obtained from particle-level ATLAS Monte Carlo samples.

The calculation provided by the authors of Ref. [42] applies to hadronically-decaying top quarks with large transverse momentum (p_{T}) in the $pp \to t\bar{t}$ process[3]. These top quarks possess a large Lorentz boost ('boosted' top quarks), and so their decay products are sufficiently collimated in the lab frame that they may be reconstructed using a single large-radius (large-R) jet [44, 45].

The theoretical advantage of reconstructing the top quark decay products as large-R jets is that soft-drop grooming, a generalisation of the modified mass-drop (mMDT) grooming [46], may be applied [47]. This procedure isolates the top quark mass dependence from the issues of non-global logarithms [48] and nonperturbative QCD effects of colour-reconnection to the underlying event (UE), enabling the calculation of jet substructure distributions in perturbative QCD to higher orders [49–55]. Such calculations have been compared to measured light-quark and gluon jet data from the LHC and RHIC by the ATLAS, CMS, ALICE and STAR collaborations; excellent agreement has been observed when non-perturbative effects are small [56–60]. More generally, it is important to account for non-perturbative QCD effects field-theoretically to obtain precise predictions [61].

This study is performed with samples where UE modelling is switched off: effects related to the UE and colour-reconnection are addressed in a dedicated section of this document.

This note is organized as follows: a brief overview of the NLL prediction is given in section 2. The Monte Carlo samples used for the study are described in section 3. The fitting procedure is outlined in section 4. Section 5 provides an overview of the main sources of uncertainty on the calibration, including a study on how UE effects may alter the m_t^{MC} and m_t^{MSR} mass relation. The main results of this study are presented in section 6. Concluding remarks and directions for future iterations of such calibrations are provided in section 7.

2 Theoretical prediction

The calibration procedure for the top quark mass parameter in MC simulation, m_t^{MC}, was proposed in Ref. [40]. This first study was based on a prediction for the particle–level hemisphere mass in $e^+e^- \to t\bar{t}$ production at high energy. The work of Ref. [42] extends the calculation to particle–level observables at hadron colliders. In this section, the most important aspects of the calculation are briefly summarized.

Soft and collinear emissions from the top quark and its decay products characterize the main features of the jet mass distribution. Sensitivity to the top quark mass through the jet mass measurement comes mainly from top quark decay products and the accompanying collinear radiation. For highly-boosted top quarks ($p_{\mathrm{T}} \gtrsim 600$ GeV) the decay products are well-contained within the large-R jet, and so the top decay can be treated inclusively[4]. For this inclusive treatment of the top quark decay products, the contribution of the

[3] An alternative approach to calibrating Monte Carlo samples has been proposed in Ref. [43], although it is not considered in these studies.

[4] ATLAS uses a right-handed coordinate system with its origin at the nominal interaction point (IP) in the centre of the detector and the z-axis along the beam pipe. The x-axis points from the IP to the centre of the LHC ring, and the y-axis points upward. Cylindrical coordinates (r, ϕ) are used in the transverse plane, ϕ being the azimuthal angle around the z-axis. The pseudorapidity is defined in terms of the polar angle θ as $\eta = -\ln\tan(\theta/2)$.

collinear radiation to the jet mass cross section can be calculated, and involves the same components at hadron colliders as in e^+e^- collisions [62, 63].

Accurately quantifying the contribution of soft radiation to the predicted large-R jet mass differential cross-section is more challenging : the soft sector includes not only soft radiation from within the jet, but also soft emissions which originate elsewhere in the event and which are uncorrelated with the top quark decay products, such as initial state radiation (ISR) and underlying event. The leading non-perturbative QCD effects on the jet mass spectrum due to hadronization also originate in the soft sector.

Jet grooming algorithms allow one to selectively groom away soft and/or wide-angled particles, reducing the undesirable effects of soft radiation on the jet mass spectrum. The particle-level calculation for the jet mass distribution from top quark decays in reference [42] incorporates soft-drop grooming for this reason. In order to maintain an inclusive treatment of the top decay products, the soft-drop grooming must not be too aggressive. At the same time, one needs a sufficient level of grooming to remove the undesirable soft/wide-angled radiation. As a result of these constraints, the region of validity of the calculation in reference [42] is demarcated by 'light-grooming' conditions: these constraints demand that the top-quark jets must be sufficiently boosted and that the soft-drop grooming must be less aggressive than what is typically considered in physics analyses with groomed jet substructure observables. An energy cut of $z_{\text{cut}} = 0.01$ is recommended, roughly an order of magnitude smaller than the typical configurations, in conjunction with a large angular-weighting parameter $\beta = 2$. When such light grooming conditions are satisfied, a perturbative calculation of the normalised jet mass spectrum becomes possible, which was presented in reference [42] for the normalised groomed jet mass cross section at NLL accuracy.

The effects of hadronisation on the groomed jet mass cross section, while reduced compared to the ungroomed jet mass, still need to be accounted for in order to achieve the desired precision. Given the nature of the soft radiation and the complex interplay with the soft drop grooming, the hadronisation corrections to the jet mass distribution depend on both the kinematic parameters such as the jet p_{T} and jet rapidity, the soft-drop parameters z_{cut} and β, and the kinematic phase space of the top decay products. In the determination of the relation between the top mass parameter in Monte Carlo simulation and the top quark mass in the NLL calculation, the grooming is applied to MC events with the same configuration as in the calculation.

A first-principles field-theoretical formalism for nonperturbative corrections to the soft-drop jet mass for jets initiated by light quarks and gluons was presented in reference [40, 61] and was generalized to the case of decaying top quarks in reference [42]. It was shown that the hadronization effects at leading power are proportional to an $O(\Lambda_{\text{QCD}})$ nonperturbative parameter, Ω_{1q}^{∞} that is independent of any kinematic and grooming parameters, as well as top decay product phase space. On the other hand, the dependence of the hadronisation correction on these variables factorizes into perturbatively-calculable coefficients. Hence, a hadron-level determination of the top mass through this observable involves two additional unknown parameters, Ω_{1q}^{∞} and x_2, where the latter accounts for hadronic corrections that are less correlated with the top quark mass. In practice, in the NLL code Ω_{1q}^{∞} is the first moment of a hadronic shape function, while x_2 is the ratio of its second cumulant to $(\Omega_{1q}^{\infty})^2$. Variations in x_2 are expected to have a milder impact on the large-R jet mass peak position than those in Ω_{1q}^{∞}.

Figure 1 shows the prediction of the calculation. The peak position of the groomed top jet mass distribution depends on the value of the top quark mass. The actual peak position is shifted due to hadronisation that depends on Ω_{1q}^{∞} and x_2. The degeneracy between the three parameters is resolved following the example of Ref. [42]: as the three perturbative coefficients of the hadronisation corrections have a different dependence on the jet p_{T}, this degeneracy is broken by a simultaneous fit to multiple p_{T} bins.

The code that implements the calculation allows the configuration of various levels of soft-drop grooming, as long as the requirements of light-grooming are satisfied. The top quark mass is specified in the scale-dependent MSR mass scheme ($m_t^{\mathrm{MSR}}(R)$) proposed in Ref. [64]. The MSR mass is a low-scale short-distance mass derived from the $\bar{M}S$ scheme, and can be regarded as a 5-flavour extension of the 6-flavour $\bar{M}S$ mass, suitable for scales R below the top quark mass [41]. With a scale choice $R = 1$ GeV, the MSR mass is numerically very close to the top quark pole mass, but the MSR mass remains free of the pole mass renormalon. All results in this note are presented in the MSR scheme, with the scale R set to 1 GeV, which yields numerical results close to the pole mass.

The uncertainty on the prediction due to missing higher-order corrections is estimated by varying several scales in the calculation. There are five scale parameters: the hard scale parameter e_H (related to the renormalisation and factorisation scales), the top mass scale parameter e_m, the general soft scale parameter e_{SG}, the top soft scale parameter e_{St} and the top-antitop jet scale parameter e_{Gt}. The five profile functions that govern these scales are varied by factors of 2 and 1/2, as in Ref. [42]. Figure 1 shows the nominal prediction and the ten scale variations which are considered, their envelope is taken as the total uncertainty, following the precedent in Ref. [42]. All large-R jet mass distributions from simulation are normalised to the NLL prediction in the fit window during the fitting procedure.

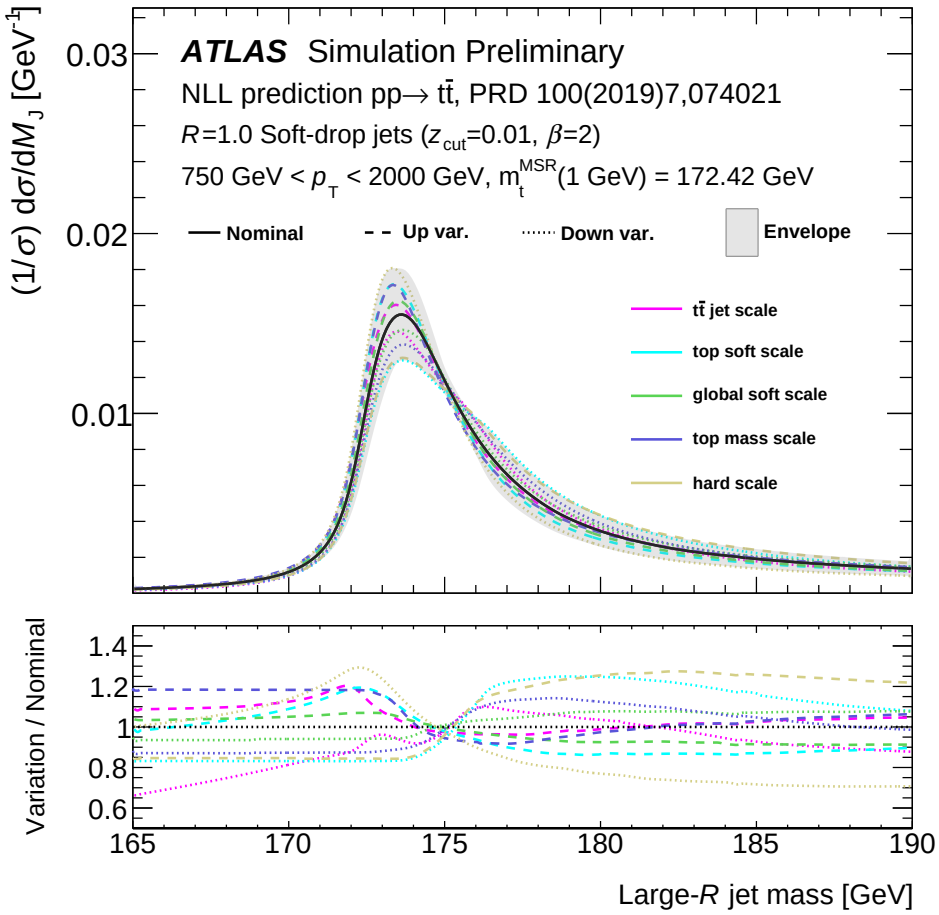

Figure 1: NLL prediction of Ref. [42] for the normalised particle-level jet mass distribution of large-R jets containing a boosted hadronic top-quark decay (black line). The coloured and dashed/dotted lines are obtained by varying the five scales in the calculation. The grey band corresponds to the envelope of all scale variations. All curves are normalized to the same area in the groomed large-R jet mass interval of 172.5–180 GeV.

3 Monte Carlo samples

The nominal ATLAS sample for top-quark pair production is generated with the NLO matrix-element event generator Powheg Box 2 [65–67] (referred to as the 'nominal' sample) with the NNPDF3.0 NLO PDF set [68]. The factorization and renormalization scales are set to $\mu_F = \mu_R = \sqrt{(m_t^2 + (p_{\mathrm{T},t}^2)}$, where the top-quark p_{T} is evaluated before it is allowed to emit radiation [69]. The matrix element generator is interfaced to Pythia v8.210 [70], and uses the A14 set of tuned parameters [71] for the parton shower, hadronisation and underlying event models. The EvtGen afterburner program [72] handles decays of b- and c-hadrons. No minimum p_{T} cut is applied to the particles used in this study. Contributions from multiple pp interactions in the same LHC bunch-crossing ('pile-up') are not included in these particle-level samples, or considered in this study.

The top quark mass parameter is set to 172.5 GeV in the nominal sample, and all other Monte Carlo samples used throughout this note. All top quarks in Monte Carlo samples are forced to decay hadronically.

A set of varied samples based on this nominal ATLAS configuration is studied in order to factorise the role played by internal settings of Pythia 8 in shaping the jet mass distribution. Such variations affect:

- the A14 tune : many Monte Carlo event generators use PS, hadronisation, and MPI models which include parameters whose values may be adjusted using fits to experimental measurements in order to more accurately generate events that model collider data. This optimisation process is known as 'tuning,' and the resulting set of parameter values are referred to as 'MC tunes.' The nominal Pythia 8 configuration in ATLAS makes use of the A14 tune [71], which was developed from ATLAS measurements of jet substructure and UE observables at $\sqrt{s} = 7$ and 8 TeV, and is nominally provided for use with the NNPDF23LO PDF set. The parameters fit in this tune are related to colour reconnection, MPI and ISR/FSR and can be grouped into subsets which are varied systematically in order to provide a good coverage of the experimental and modelling uncertainties implicit in the tuning. They are called eigentunes and are labelled as Var1, Var2, Var3a, Var3b and Var3c. Var1 is devoted to the modelling of UE effects, whilst the others are related to ISR/FSR. The impact of these tune variations on the shape of the jet mass distribution are evaluated.
- the h_{damp} parameter : this parameter is involved in the matrix-element-to-parton-shower matching, setting the cutoff scale for the first gluon emission. The value of h_{damp} for these studies was chosen to be equal to $(3/2)m_t$. Events with $h_{\text{damp}} = 3m_t$ are also studied.
- the matrix-element correction, related to the matrix-element-to-parton-shower matching, is switched off in a dedicated sample [73]. This disables matrix element corrections to the first emission in the parton shower.

The effects of initial- and final-state radiation are studied with alternative Powheg+Pythia 8 samples. A sample obtained with $h_{\text{damp}} = 3m_t$, $\mu_R = \mu_F$ reduced to half the default value, and the A14 Var3c 'up' variation produces increased amounts of radiation. A sample with $h_{\text{damp}} = (3/2)m_t$, $\mu_R = \mu_F$ increased to double the default value, and the A14 Var3c 'down' variation yields decreased amounts of radiation [69].

Alternative $t\bar{t}$ simulations are used to assess variations in the definition of the top mass among MC programmes. The Powheg generator interfaced to Herwig 7 [24] (v7.1.3) with the H7UE tune provides alternative models for the parton shower, underlying event and hadronisation. The MadGraph5_aMC@NLO v2.3.3.p1 generator [74] provides an alternative matrix-element calculation. This matrix-element calculation is interfaced to Pythia 8 with the same settings as the nominal Powheg sample, and the same renormalisation and factorisation scales are also used.

Several further samples were used to validate certain aspects of the Monte Carlo generation or to test the impact of generator settings:

- Recoil-to-coloured setting: the way recoils to coloured objects and colour singlets are treated in the parton shower may affect the jet mass distribution. To study this effect, two MC samples that differ only in the choice of the "recoil-to-coloured" switch in Pythia 8 are considered. By default, this switch is set to "ON" in Pythia 8, but recent studies show that "OFF" may be an equally plausible choice [30].
- The value of the *rFacB* parameter which controls the longitudinal momentum sharing of B hadrons in the string-based hadronisation model used in Pythia 8. Lower values of *rFacB* give rise to softer B spectra. For this study it is varied from its default value of 0.65 to 1.05, replicating the strategy adopted in the ATLAS $t\bar{t}$ modelling uncertainties prescription [73].

- By default, Pythia 8 is interfaced with EvtGen to handle the decay of B and D hadrons. A dedicated sample without EvtGen is considered as well.

4 Methodology

The jet mass distribution from Monte Carlo simulation (section 3) is obtained for particle-level jets by clustering all stable final-state particles produced by the generators (equivalent to Pythia status code 1). By default, these final-state particles are produced by the hadronisation algorithm of a Monte Carlo generator. By disabling the hadronisation algorithms (*e.g.* by disabling the 'HadronLevel:all' switch in Pythia 8), the set of final-state particles instead corresponds to a set of partons produced in the hard scattering and parton shower; this parton-level picture is used in some studies presented in sections 4.1 and 4.2.

The nominal jet reconstruction algorithm used is the XCone algorithm with $\beta = 2$, $\gamma = 2$ and radius parameter $R = 1$ [75], as implemented in FastJet [76]. The anti-k_t recombination algorithm [77] is also studied, with the same radius parameter. Soft-drop grooming with parameter values $\beta = 0, 1$ or 2 and $z_{\text{cut}} = 0.01$ or 0.05 is applied in order to remove soft– and wide–angled contributions to the jet.

A simple event selection is applied to the Monte Carlo simulated events. Events are required to contain at least one large-R jet with a p_{T} above 750 GeV. This jet is matched to the top/anti-top parton after emitting final-state radiation (FSR), but before the top decays, by requiring $\Delta R(\text{jet,top}) < 1.0$. In order to avoid pathological configurations where two large-R jets overlap (which cannot be compared to the theory prediction) the leading and subleading large-R jets must be separated by a distance of $\Delta R > 1.0$.

4.1 The jet mass in high-p_{T} top decays

The evolution of the jet mass lineshape from parton-level to particle-level is considered in this section by sequentially enabling aspects of the Pythia simulation including FSR from the top quark decay products, the parton shower, hadronisation and the underlying event.

Figure 2 shows the jet mass distribution for XCone jets with $R = 1$ and ungroomed jet p_{T} between 0.75–2 TeV, produced by the nominal Pythia 8 Monte Carlo generator setup with a top-quark mass of $m_t^{\text{MC}} = 172.5$ GeV. The results in Figure 2(a) correspond to ungroomed jets, and those in Figure 2(b) to jets groomed with the soft-drop algorithm configured using the 'light-grooming' settings, $\beta = 2$ and $z_{\text{cut}} = 0.01$.

A comparison of the four histograms in each figure shows how the different stages of the Monte Carlo generator transform the jet mass distribution. The histogram represented by the black line shows the jet mass distribution at parton-level after the parton shower that is obtained when the Underlying Event model is switched off. Final-state-radiation from top decay products is disabled here using the Pythia 8 switch "FSRinResonances" (we will use the notation "FSRinRes=off" as a shorthand), which allows final-state radiation from the top quark itself, but prevents top quark decay products from radiating. Hadronization, as well as radiation off of the top quarks and emissions in the parton shower cause a significant tail at large values of the jet mass. A comparison of Figure 2(a) and Figure 2(b) shows that grooming reduces sensitivity to haronisation and the underlying event, improving the top jet mass resolution. Even with the light grooming settings used here, the high-mass tail is reduced significantly.

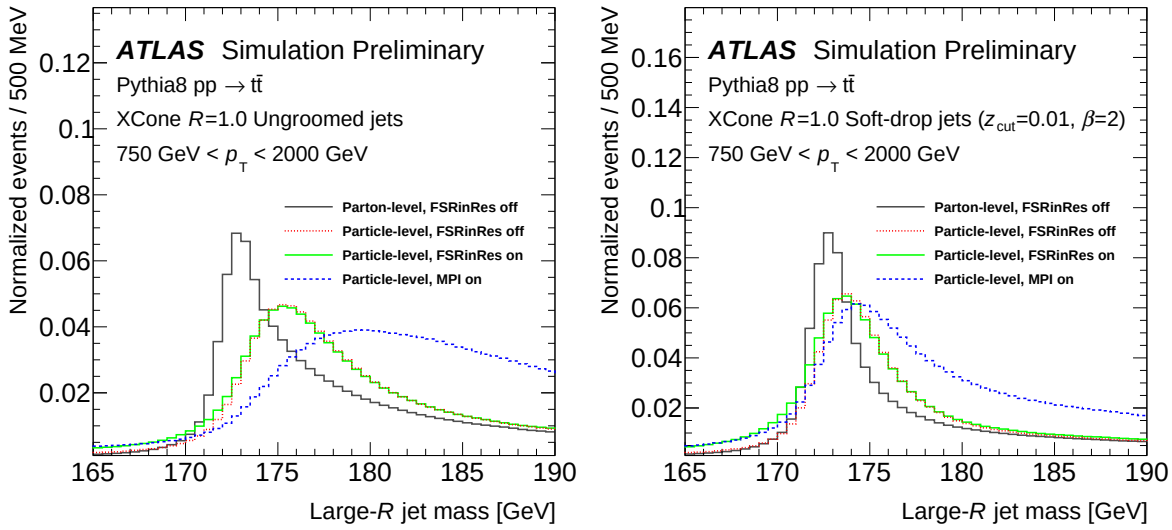

(a) (b)

Figure 2: Large-R jet mass distributions obtained from the reference Pythia 8 setup for (a) ungroomed XCone jets with $R = 1$ and (b) the same jets after applying a 'light' soft-drop grooming ($\beta = 2$, $z_{\text{cut}} = 0.01$). Different levels of Monte Carlo simulation at parton- and particle-level are shown, where the labels FSR and MPI respectively indicate whether final state radiation in resonances and multi-parton interactions (*i.e.* underlying event) are activated in the simulation.

The effect of hadronisation becomes clear by comparing such configuration at parton- and particle-level. In the ungroomed case, the distribution is profoundly altered: the top-mass peak is smeared and shifted by more than 3.5 GeV. Light grooming reduces the impact of the hadronisation, limiting the shift of the peak to approximately 1.5 GeV.

In the case where the FSR in resonance decays is switched on, while the MPI is still off (labelled 'FSRinRes on' in the figure), this effect leaves the peak position unaltered, but has an effect on the low-mass tail, as wide-angle emissions from the top decay products can escape the catchment area of the jet. This effect is most clear for groomed jets, which have an increased sensitivity to the top decay products and their radiation.

When the UE modelling is turned on ('MPI-on'), the additional radiation that falls on the jet catchment area has the effect of further broadening the distribution and lifting up the high-mass tail. The impact is most pronounced for the ungroomed jets, where the top mass peak is smeared out over a broad mass range between 175 GeV and 195 GeV. Grooming effectively mitigates the impact of UE on the jet mass distribution. The shift of the peak position in the particle-level result when UE is toggled on/off is less than 0.8 GeV.

4.2 Template-fitting procedure

A χ^2-minimization is carried out to find the values of parameters in the theoretical calculation at NLL (section 2) that best describe the Monte Carlo predictions (section 3). Templates are produced with the NLL calculation in a fine grid of values of the three parameters: $m_t^{\text{MSR}}(R = 1\text{ GeV})$ between 171.0 GeV and

174.0 GeV with 0.05 GeV steps, Ω_{1q}^{∞} between 0.1 GeV and 4.0 GeV in 0.1 GeV steps, and x_2 between 0.02 and 1.0 with steps of 0.02. In total, 2.3 million templates are produced. For each point, the χ^2 is calculated using the normalized NLL and MC predictions, as a function of the three scanned parameters and considering the MC statistical uncertainty.

To obtain the central value and uncertainty for each parameter, the χ^2 distribution is marginalized by scanning the values of the other parameters and finding the lowest χ^2 value. This procedure is repeated for all values of the parameter of interest and the best-fit value is estimated from the one-dimensional marginalized χ^2 distribution. The best estimate for a given parameter is taken as the value which minimizes the χ^2 distribution, and its associated uncertainty is delimited by those values of the parameter that lead to an increase of the χ^2 by 1 unit with respect to the minimum.

Both the preferred value of the parameter and its uncertainty are obtained by fitting the marginalised χ^2 distributions to second-order polynomial functions. The total 3D χ^2 comes from a combination of fits performed on the large-R jet mass distribution in three bins of the ungroomed large-R jet p_{T}, following the approach taken in Ref. [42] in order to disentangle the non-perturbative parameter behaviour from the behaviour of m_t^{MSR}. The following three p_{T} intervals are considered in the determination of the MSR and MC mass relation: 750 GeV $< p_{\mathrm{T}} <$ 1 TeV, 1 TeV $< p_{\mathrm{T}} <$ 1.5 TeV and 1.5 TeV $< p_{\mathrm{T}} <$ 2 TeV.

To assess the level of agreement between the best-fit calculation (Section 2) and the Monte Carlo simulation, they are compared in Figure 3. The top-quark mass parameter is set to $m_t^{\mathrm{MC}} = 172.5$ GeV in the Monte Carlo generator. The range of groomed large-R jet masses included in these fits is always taken to be between 170-180 GeV.

In figure 3(a), the comparison is performed at parton level, *i.e.,* without FSR in resonance decays, hadronisation or UE in Pythia 8. The parton-level NLL calculation has only one free parameter, the MSR top-quark mass, which is adjusted with a χ^2 minimization. The histogram in Figure 3(a) corresponds to the mass values that give the best agreement: $m_t^{\mathrm{MSR}} = 172.75$ GeV. The results are in good agreement; the theory prediction lies on top of the Monte Carlo generator result over a wide mass range around the peak. Any deviations in the shape are well within the theory uncertainties, represented by the gray band and calculated as explained in section 2.

In figure 3(b) the results of the NLL calculation and the Monte Carlo generator are compared at particle level, but with FSR in resonance decays still disabled. The effect of the hadronisation model on the Monte Carlo generator is to shift and smear the top mass peak. The NLL calculation includes the effect of hadronisation in the form of a shape function with two parameters, as described in section 2. The top mass and the two additional degrees of freedom are adjusted in a three-dimensional fit. The best-fit curves again provide an adequate description of the Monte Carlo generator prediction.

Finally, FSR from top decay products is activated in the Monte Carlo generator. Some of the radiation is groomed away, leading to changes in the low-mass tail under the top mass peak, as discussed in Section 4.1. In Figure 3(c) the result is compared to the best-fit result of the calculation. Even with three free parameters, discrepencies arise between the jet mass distributions of the theory and simulation which cause the χ^2/NDF value to increase. These differences arise particularly because the theory treats top decay products inclusively, it does not allow for the possibility of radiation from the top decay products to be groomed during the soft-drop procedure. As the relation between the MC mass and the MSR mass is determined with FSR in resonance decays switched on, a careful treatment of the low-mass tail is necessary.

Figure 3(d) shows a comparison between the NLL calculation and the Monte Carlo generator at particle level, with the underlying event model enabled in simulation. The effects of the underlying event increase the tail at high values of the groomed jet mass, and are partially absorbed by the soft shape function in the NLL prediction. While the mass distribution in this figure shows adequate agreement, the scaling of the soft function with jet p_{T} and radius in the NLL prediction is not presently accurate enough for use in the calibration procedure. Calibration fits with the UE enabled are not pursued in the current iteration of these studies.

The value of the MSR mass extracted from fits to Figure 3(a) is largely independent from the mass region considered in the fit. That is no longer true when fitting with FSR in resonance decays and hadronisation activated (Figure 3(c)). The calculation fails to describe the tail below the top mass peak that is present in the generator prediction. This is again related to to the inclusive treatment of top decay products in the theory prediction: as these contributions cannot participate in the grooming procedure, the theory does not accurately describe the low-mass tail that is present in the generator prediction. The discrepancy in the low-mass tail limits the theory prediction's range of validity. A fit that includes the low-large-R-jet-mass tail will bias the extracted top mass to lower values. Therefore, the jet mass window where theory and simulation are compared needs to be carefully adjusted in order to provide a reliable relation between the mass parameter in the generator and the m_t^{MSR} in the calculation.

Figure 4 shows the dependence of the best-fit χ^2 value on the choice of the lower limit of the fit range, along with the statistical uncertainty. When fit ranges start at low masses, the discrepant low-mass tail is included, causing the χ^2 value to increase. When fit ranges start at high values, the peak region is not included and the statistical uncertainty on the top-quark mass parameter increases very rapidly. The lower limit of the fit range is therefore set to the lowest possible value in the χ^2 plateau. In practice, this is achieved by setting the lower limit of the fit range to the mass parameter of the Monte Carlo generator. This choice ensures that the mass peak, which sits 1.5 GeV above the MC mass parameter, is properly included (even in samples with a shifted mass). Consequently, the large-R jet mass range used in the calibration fits is between 172.5 GeV–180 GeV. An uncertainty associated with the choice of the large-R jet mass range used in the fit is discussed in section 5.2.

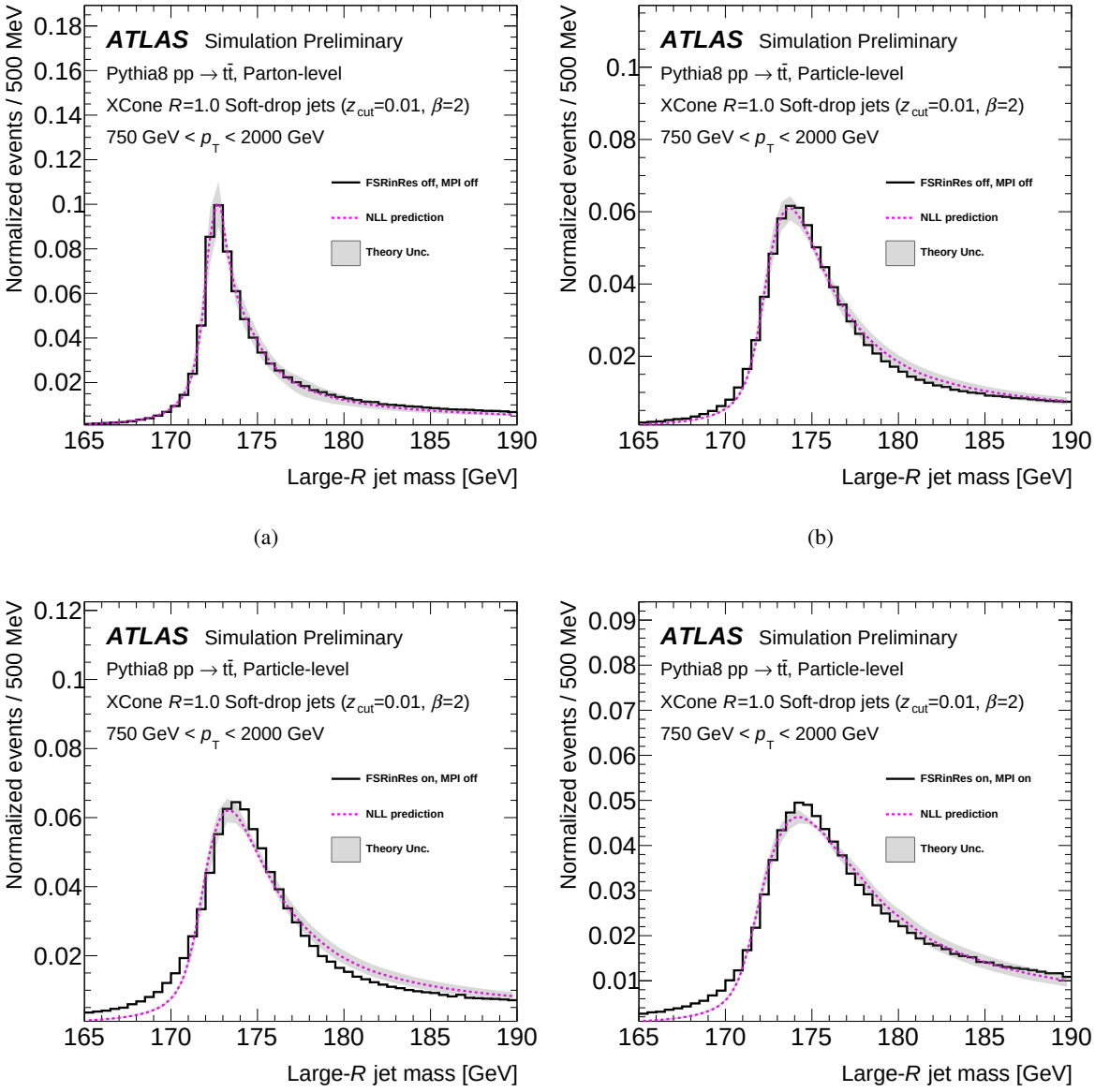

Figure 3: Comparison of the NLL prediction of Ref. [42] to several PYTHIA 8 predictions with $m_t^{\mathrm{MC}} = 172.5$ GeV. The distributions correspond to (a) the MC and NLL predictions at parton-level and with FSR in resonance decays (PYTHIA 8 setting 'FSRinRes') turned off, (b) the particle-level prediction with FSRinRes and Underlying Event modelling (PYTHIA 8 setting 'MPI') turned off, (c) the particle-level predictions with FSRinRes turned on and MPI switched off, and (d) the particle-level predictions with FSRinRes and MPI turned on. The distributions are normalized and the fit is performed on the interval 170 GeV $< m_J <$ 180 GeV, where m_J is the large-R jet mass. Fits are performed in three bins of the ungroomed large-R jet p_{T}; these figures are shown in a single p_{T} bin for illustrative purposes.

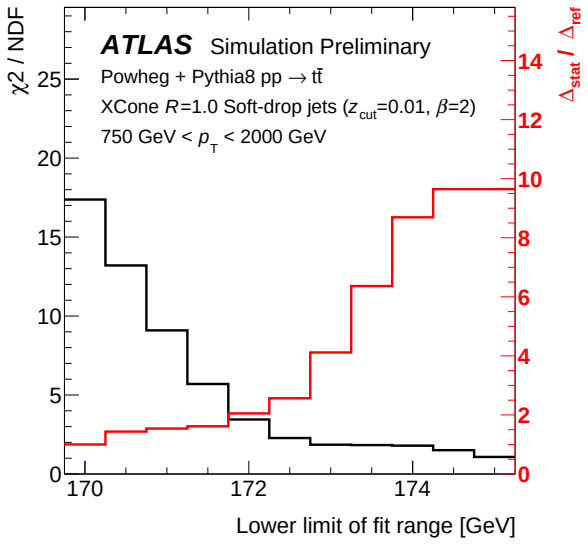

Figure 4: The χ^2 value and the statistical uncertainty obtained from a fit with the NLL calculation of Ref. [42] to a Monte Carlo prediction at particle level, as a function of the lower limit of the fit. The statistical uncertainty is described in terms of the relative uncertainty of the full sample (Δ_{ref}) to the uncertainty after cutting on the the lower-limit of the fit range (Δ_{stat}). The Monte Carlo prediction is based on Pythia 8 with a top quark mass of 172.5 GeV. MPI is turned off, Final State Radiation in resonances is turned on in the Monte Carlo.

5 Uncertainties

This section provides a description of sources of uncertainty on the relation between the MC mass and the MSR mass for a given observable and Monte Carlo generator setup. Theory uncertainties are estimated in Section 5.1 and uncertainties related to the methodology in Section 5.2, and the impact of uncertainties on the UE model is estimated in Section 5.3.

5.1 Theory uncertainty from scale variations

The estimate of uncertainty due to missing higher-order corrections in the calculation is based on the scale variations illustrated in figure 1. Alternative theory predictions are generated for the ten scale variations. The three parameters, m_t^{MSR}, Ω_{1q}^{∞} and x_2, are set to the best-fit values obtained in a fit to the nominal ATLAS Monte Carlo prediction with Powheg +Pythia 8. The NLL prediction with the default scales, is then fit to each of the alternative predictions, with the three parameters freely floating. In this way, the impact of the theory uncertainty on the mass relation is estimated.

Figure 5 presents the fit results for the ten scale variations. The total uncertainty is taken as the difference of the fitted mass value and the nominal results. For most scale variations the MSR mass is shifted by less than ±200 MeV. The largest deviations come from variations of the soft and jet scale parameters. The total theory uncertainty is taken as the envelope of the ten scale variations, following the prescription in Ref. [42]. In the MSR scheme it amounts to +230 MeV in the positive and −310 MeV in the negative direction. The same exercise is repeated in the pole scheme, leading to a slightly smaller variation of the mass: +150 MeV and −250 MeV.

The size of the scale uncertainty is similar to the result reported for the calculation at NLL accuracy of the 2-jettiness in electron-positron collisions in Ref. [41]. The theory uncertainty is expected to decrease as the formal accuracy of the calculation increases in the future. Ref. [41] observes an important reduction of the uncertainty from NLL to NNLL, and from NNLL to N^{3}LL. Assuming a similar convergence in the hadron collider environment, the scale uncertainty could be reduced to approximately half of the current value with an NNLL calculation, and to a quarter at N^{3}LL.

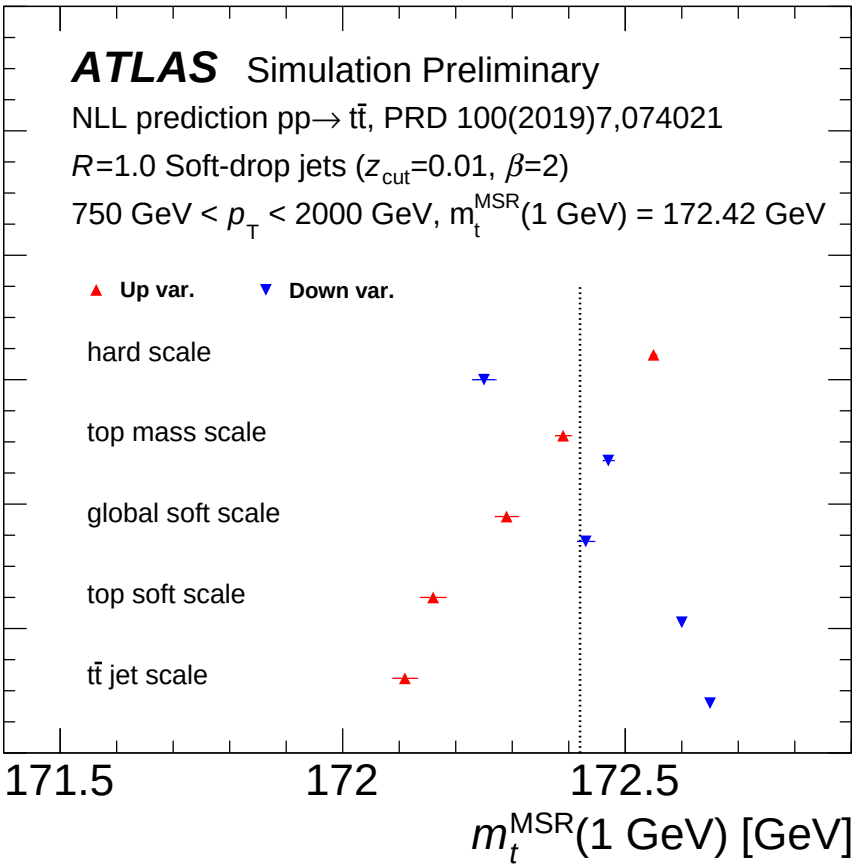

Figure 5: Impact of scale variations in the NLL calculation expressed in terms of the top quark MSR mass. The values of m_t^{MSR} are found by fitting the nominal NLL calculation to the predictions obtained with different choices of the five scales. The three parameters of the calculation are floated in the fit. For the calculations with alternative scale choices the parameters are set to the best-fit values for the ATLAS Powheg +Pythia 8 sample: $m_t^{\mathrm{MSR}}(1\ \mathrm{GeV}) = 172.42$ GeV (indicated by a vertical line), $\Omega_{1q}^{\infty} = 1.49$ GeV, $x_2 = 0.52$.

5.2 Method uncertainties

The fit result depends on certain choices made in the fit method. The most important ones are the choice of the fit range and the kinematic ranges that are considered in the fit. Uncertainties are assigned to cover any potential bias of the mass relation due to these choices.

The impact of the choice of the mass range in the fit is evaluated by varying the lower limit, as described

in section 4. Theory-to-MC comparisons are carried out in two alternative jet mass ranges, beginning at 172.0 GeV or 173.0 GeV. The fit range extends up to 180 GeV in all cases. In this exercise the value of x_2 is limited to ±0.1 around the best-fit result, to avoid excessive instability of the fit. The MSR mass values obtained from the fits with alternative mass ranges are compared to the nominal fit result and the difference is assigned as an uncertainty. This results in an uncertainty of ±170 MeV. Similar variations in the upper edge of the fit range by ±1 GeV result in variations of the result by ±30 MeV.

The impact of the choice of the large-R jet p_{T} intervals included in the fit is evaluated by comparing fits on subsets of two p_{T} bins. The fit is repeated on all permutations of two out of three intervals defined in Sec.4.2, and compared to the nominal fit, that has all three bins. The maximal variation, ±80 MeV, is taken as the uncertainty.

These two components are added in quadrature, resulting in a combined methodological uncertainty of 190 MeV.

5.3 Underlying event and colour-reconnection modelling

As multi-parton interactions are switched off in the samples used to determine the relations between the MC mass and the MSR mass in section 6, the effect of Underlying Event modelling on the large-R jet mass distribution must be accounted for separately. The uncertainty on the UE contribution is estimated using the A14 Var1 variations, and by changing the colour-reconnection models available in Pythia 8.

Given that the NLL prediction does not include effects related to the UE, an alternative approach has to be taken in order to provide an estimation of the position of the top jet mass peak. A robust fit is obtained with the 'template method', where particle-level templates for arbitrary mass values are created with a Breit-Wigner reweighting of the parton-level top mass distribution in the nominal ATLAS Monte Carlo sample. The best-fit mass parameter corresponding to any of the alternative samples is then found by a χ^2 minimization.

The Underlying Event modelling is varied in samples generated with Pythia 8, with multi-parton interactions switched on (MPI=on). Figure 6(a) presents the top jet mass distributions for the nominal sample with MPI=on, and two variations of the A14 tune. The sample with MPI=off is presented for reference. The impact of the MPI is a clear shift of the top mass peak to larger values. The distribution is also smeared out considerably. The A14 Var1 'up' and 'down' variations [71] tune variations change the UE activity by varying the BeamRemnants:reconnectRange parameter in Pythia8 from 1.73 (up) to 1.69 (down) (the nominal value is 1.71), and the MultipartonInteractions:alphaSvalue from 0.131 (up) to 0.121 (down), (the nominal value for α_s in the MPI model from NNPDF is 0.126). These variations alter the large-R jet mass distribution : the Var1-up mass spectrum is harder and the Var1-down mass spectrum softer than the nominal A14 distribution.

The template-fit method yields values of m_t^{MC}= 172.64 ± 0.008 GeV and 172.34 ± 0.007 GeV for the up and down A14 variations, respectively, where the uncertainty corresponds to the MC statistical uncertainty. The difference with respect to the MC mass value used in the nominal template, m_t^{MC} = 172.5 GeV, is taken as an uncertainty, resulting in a symmetrized UE uncertainty of ±150 MeV.

Several alternative colour reconnection (CR) models available in Pythia 8 are also studied, and compared to the scenario where the color-reconnection setting is off. The large-R jet mass distributions associated to these options are compared to the default Pythia 8 MPI-based colour-reconnection model ('CR0') in figure 6(b). The first alternative model ('CR1') is based on QCD colour rules and is observed to produce

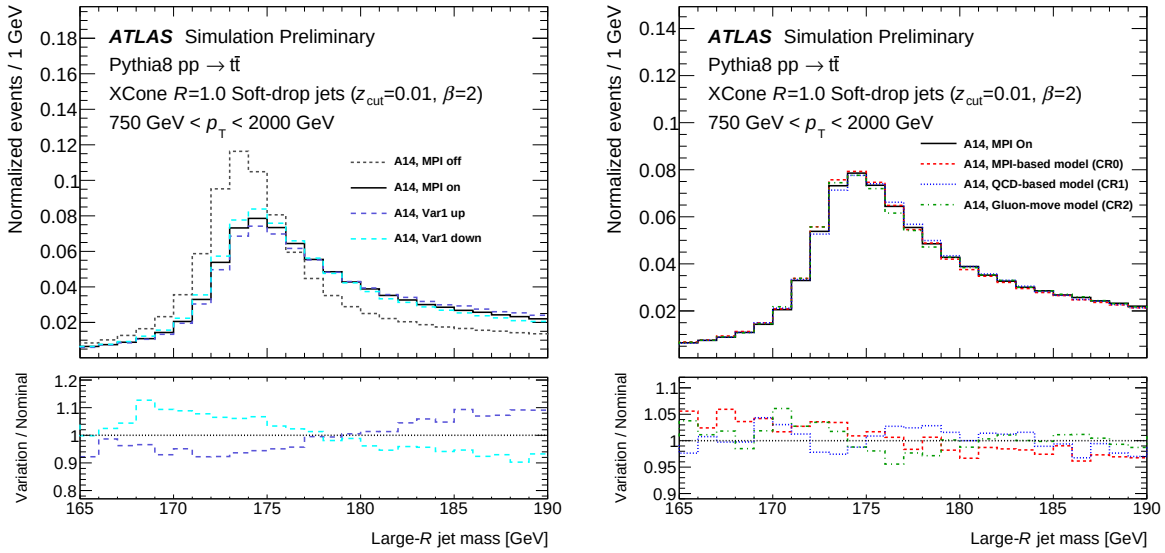

Figure 6: The large-R jet mass for boosted, hadronically-decaying top quarks for (left) the Pythia 8 A14var1 up and down variations and (right) several colour-reconnection models available in Pythia 8. For reference, the distribution is also shown for the nominal A14 tune, and with multi-parton interactions disabled in the left panel. Large-R jets are reconstructed using the XCone algorithm and light soft-drop grooming.

more massive jets, while the second alternative model ('CR2') which is based on the gluon-move scheme produces fewer massive jets. The associated m_t^{MC} values for the different colour-reconnection models are 172.52 ± 0.01 GeV and 172.44 ± 0.01 GeV, respectively. The colour reconnection uncertainty is -60 MeV and $+20$ MeV.

The contributions from UE and CR modelling are added in quadrature and symmetrized to yield a total uncertainty of ± 155 MeV.

5.4 Summary of uncertainties

The uncertainties on the relation between the top quark mass parameter in Monte Carlo event generators and the MSR mass scheme $m_t^{\mathrm{MSR}}(1\ \mathrm{GeV})$ are summarized in Table 1.

Table 1: Uncertainties on the relation between the top quark mass parameter in Monte Carlo generators and the MSR mass at a scale of 1 GeV.

Source	**Size [MeV]**	**Comment**
Theory (higher-order corrections)	$+230/-310$	Envelope of NLL scale variations
Fit methodology	± 190	Choice of fit range, p_{T} bins
Underlying Event model	± 155	A14 eigentune variations, CR models
Total Systematic	**$+340/-340$**	
Statistical Uncertainty	± 100	
Total Uncertainty	**$+350/-410$**	

These uncertainties apply to the mass relation for a given Monte Carlo generator setup. Variations of the parton shower and hadronization model and their parameters are not considered uncertainties. The relation between MC mass parameter and the MSR mass scheme can be determined for each generator setup. Results for several of the ATLAS samples used in direct mass measurements are presented in section 6, and the impact of a larger set of variations is estimated in MC-to-MC fits.

These uncertainties are stricly valid only for the large-R jet mass, that is used to derive the mass relation. The stability of the result under variations of the observables is studied, within the limitations of the NLL calculations, in section 6. Additional uncertainties due to the extrapolation to a different observable and selection may be required if the mass relation is used to calibrate direct mass measurement that use a different set of observables.

6 Results

In this section, the main results of this note are presented. The impact of varying aspects of the Monte Carlo generation scheme on the top jet mass distribution is studied by using alternative generators and samples. The relation between the top mass parameter of the Monte Carlo generator and the MSR and top pole mass is then determined:

$$m_t^{\mathrm{MC}} = m_t^{\mathrm{MSR}}(1\ \mathrm{GeV}) + \Delta_m^{\mathrm{MSR}}.$$

The value of Δ_m^{MSR} is determined for the nominal $pp \to t\bar{t}$ generator setup used in ATLAS top physics analyses, Powheg +Pythia 8, and for several variations of the nominal Monte Carlo generator. Additional fits are performed with a varied parton shower model using a sample generated with Powheg +Herwig 7, and with varied matrix element calculations implemented in a MC@NLO +Pythia 8 sample. The underlying event model is switched off for all Monte Carlo samples considered in these fits.

6.1 Impact of Monte Carlo generator variations

The impact of a complete set of Monte Carlo variations is obtained using MC template fits. In these fits Monte Carlo templates for the nominal ATLAS sample, with a floating mass parameter, are compared to alternative Monte Carlo generator setups.

Standalone Pythia 8 with the Monash tune

Ref. [42] studied Pythia 8 (version 8.240) with the Monash tune. For reference, the shift of the top quark mass parameter was determined in the nominal ATLAS Powheg + Pythia 8 sample with an MC-to-MC template fit. This yields a mass shift of +50 MeV. The slight shift is entirely due to the change of tune: the mass shift reduces to 0 if the A14 tune [71] is used.

Matrix Element variation

A template fit is performed to MadGraph5_aMC@NLO +Pythia 8 sample, yielding a MC mass of 172.44 ± 0.03 (stat.) GeV. In order to isolate the effect of the ME-PS matching, the result must be compared to a Powheg +Pythia 8 with the Matrix Element corrections in Pythia 8 switched off. An MC mass of 172.40 ± 0.04 (stat.) GeV was found for this sample. The effect of replacing the nominal Matrix Element generator in ATLAS MC samples, Powheg by the alternative MadGraph5_aMC@NLO has a negligible

effect in terms of the MC mass, given the uncertainties of the template fits. Matrix element corrections themselves do introduce a shift of 100 MeV on the MC mass.

Tune variations

Figure 7 compares the large-R jet mass distribution for each of the A14 eigentunes [71]. The Var2, Var3a, Var3b vary parameters related to the emission of additional jets (ISR or FSR), like the α_s value in time-like showers and the reference p_T of space-like showers. Var3c modifies the α_s value in space-like showers and affects only initial-state-radiation. The shape of the jet mass distribution is observed to change for the tune variations that affect final state radiation and is insensitive to Var3c, as expected.

The mass shifts corresponding to each of these variations are summarized in Figure 8. The A14 variations Var2, Var3a and Var3b lead to a mass shift of up to ±150 MeV and are generally symmetric for the up and down variations.

An advantage of the MC-to-MC template fit is that it can be performed also in events with Underlying Event. The results for the eigentunes of Figure 8 can thus be compared with those obtained in the corresponding Monte Carlo samples with Underlying Event modelling switched on. For the Var2, and Var3 variations the pattern of mass shifts is very similar for MPI=on and MPI=off. Most results agree to within 20 MeV and all are within 50 MeV. The relation between the MSR mass and MC mass derived in Monte Carlo sample without the Underlying Event therefore appears to be a good indication of how the mass definition evolves with the parton shower, even if the Underlying Event model may further modify the mass relation.

The results for a few further alternative $t\bar{t}$ samples listed in section 3 are also displayed in figure 11. The effect of the EvtGen package is found to be negligible, while variations of the recoil-to-colour setting, matrix element corrections and the h_{damp} variation are of the order of 100 MeV. The effect of these settings on the top jet mass is relatively small compared to its impact in observables used in direct mass measurements, such as m_{bl} in resolved $t\bar{t}$ events. The groomed jet mass is a very inclusive observable, as only very-wide-angle radiation can escape the catchment area of the large-R jet. The effect of these settings in ungroomed jets is found to be even smaller, providing further support for this explanation.

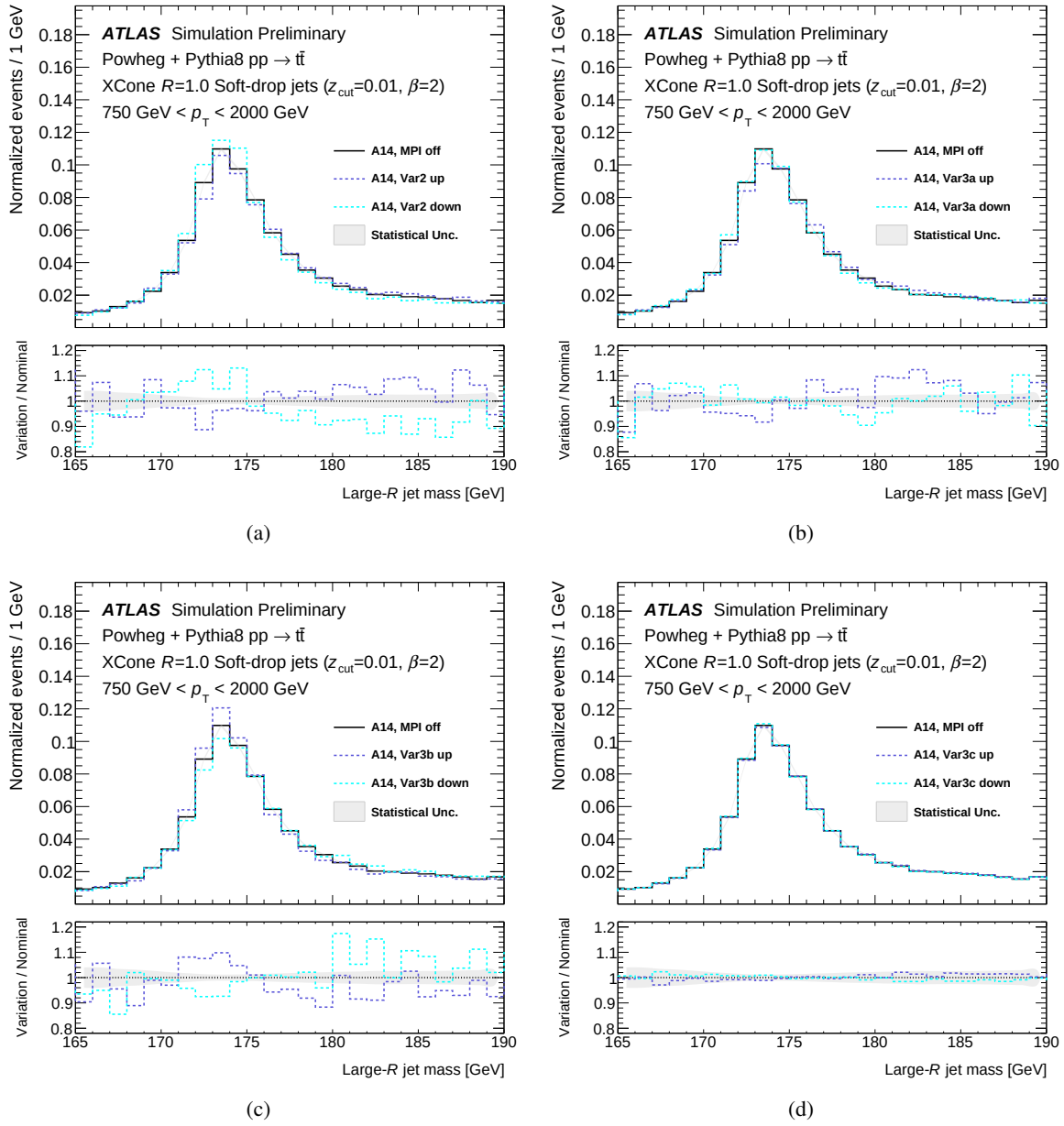

Figure 7: The large-R jet mass distributions for boosted, hadronically-decaying top quarks. Results are shown for $t\bar{t}$ events generated with POWHEG + PYTHIA 8 with Underlying Event modelling (PYTHIA 8 parameter 'MPI') switched off. Several variations of the A14 tune are shown along with the nominal setup, Var2 in panel (a), Var3a in panel (b), Var3b in panel (c) and Var3c in panel (d).

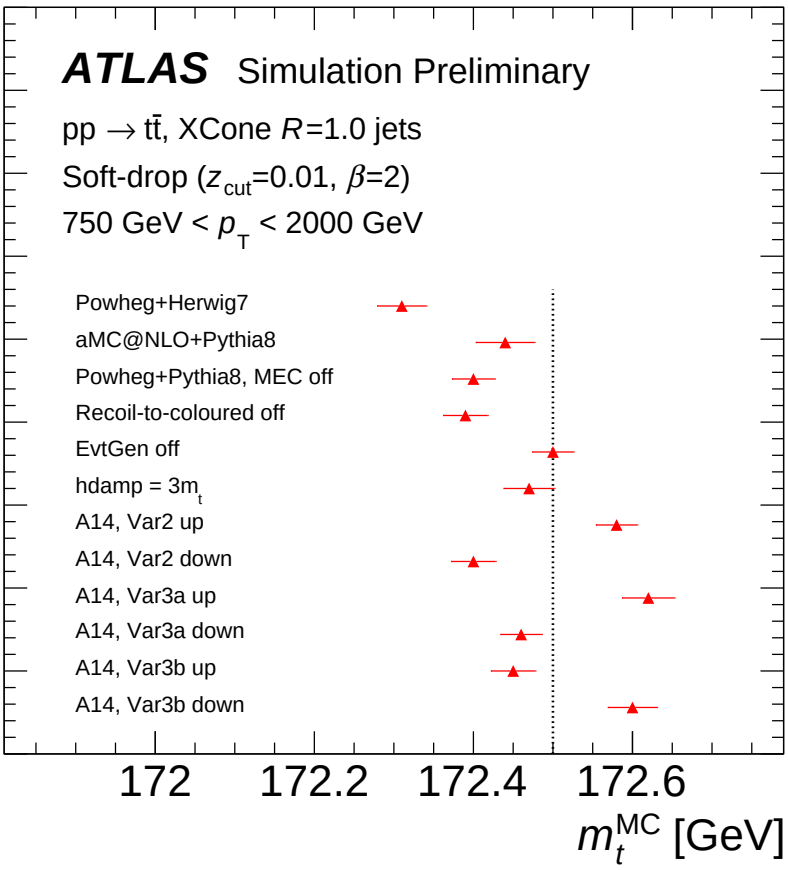

Figure 8: Equivalent shifts in the Monte Carlo mass with respect to the nominal Powheg +Pythia 8 Monte Carlo sample. The offsets are found by fitting the nominal MC mass template with a floating MC mass parameter to several alternative choices of the Powheg +Pythia 8 configuration and to the Powheg +Herwig 7 and MadGraph5_aMC@NLO +Pythia 8 samples. The underlying event model is disabled in these fits.

6.2 MC mass interpretation for the ATLAS Powheg +Pythia 8 sample

We are now ready to present the main result of this note. Figure 9 shows the normalized jet mass distributions in the three p_{T} intervals for the nominal ATLAS $t\bar{t}$ sample, generated with Powheg+Pythia 8. The best-fit NLL predictions are compared to the Monte Carlo prediction in the same figure. The NLL calculation is able to describe the main shape of the Monte Carlo prediction over the mass range and p_{T} bins included in the fit, well within the theory uncertainty band.

The best-fit result is obtained as follows. The three parameters of the NLL calculation are optimized in a global χ^2 minimization, that adds up the contributions from the three p_{T} bins. The χ^2 is based on the statistical uncertainty of the MC events, and ignores correlations due to the normalization and the theory uncertainty. The reduced χ^2 (normalized to the number of degrees of freedom) is 2.3, which is considered adequate for the purpose of this study. The linearity of the calibration procedure was confirmed by testing the fit with samples where the value of m_t^{MC} was varied between 171.5 GeV and 173.5 GeV.

The χ^2 normalized to the number of degrees of freedom is shown as a function of the three fit parameters

in Figure 10. For each pair of parameters the two-dimensional distribution is obtained by marginalizing over the third parameter. The three parameters remain highly correlated even in the fit to three p_{T} bins, as the degeneracy is only lifted partiallly by the different scaling with p_{T}.

The marginalized results for the MSR mass, Ω_{1q}^{∞} and x_2 are given by:

$$m_t^{MSR}(R = 1\ \mathrm{GeV}) = 172.42 \pm 0.10\ \mathrm{GeV},\ \ \Omega_{1q}^{\infty} = 1.49 \pm 0.03\ \mathrm{GeV},\ \ x_2 = 0.52 \pm 0.09,$$

where the associated uncertainty corresponds to the statistical uncertainty due to the limited Monte Carlo sample.

The relation between the MSR mass and the Monte Carlo mass parameter is obtained by fitting the particle-level MC prediction without Underlying Event modelling (*i.e.* MPI=off, but FSRinRES=on) :

$$m_t^{\mathrm{MC}} = m_t^{\mathrm{MSR}}(1\ \mathrm{GeV}) + 80^{+350}_{-410}\ \mathrm{MeV}, \tag{1}$$

where the uncertainty includes a statistical contribution (±100 MeV) and systematic contributions due to missing higher orders in the NLL calculation (+230/−310 MeV), due to the uncertainty associated to the fit methodology (±190 MeV), and due to the Underlying Event uncertainty (±155 MeV). The MC mass is compatible, with the MSR mass, given the uncertainty.

The MSR mass is numerically close to the top quark pole mass, within the intrinsic uncertainty of 140 MeV due to the pole mass renormalon ambiguity. Therefore, the pole mass interpretation of the MC mass parameter is validated to ∼ 0.5 GeV, the precision that is usually assigned to this identification [20].

Carrying out fits with a pole mass parameter (as opposed to the scale dependent MSR mass) in the NLL predictions, a mass relation is obtained that can be compared to the equivalent fits in Ref. [42]:

$$m_t^{\mathrm{MC}} = m_t^{\mathrm{pole}} + 350^{+300}_{-360}\ \mathrm{MeV}, \tag{2}$$

where the uncertainty is calculated in the same way as for Eq. 1. The scale uncertainties determined in Section 5 are slightly smaller for the fixed pole mass than for the MSR mass, as the MSR mass dependence on the scale R allows it to assess a source of uncertainty that is not assessed by scale variations for the pole mass.

6.3 Internal variations in the nominal sample

To determine the modelling uncertainties of ATLAS top physics analyses, many aspects of the $t\bar{t}$ production process and the hadronization are varied in variations of the nominal sample. These variations are accessible via reweighting of the nominal Monte Carlo sample. The fit between the jet mass distribution and the NLL prediction were repeated for all variations.

The results are shown in figure 11. The alternative models include variations of the value of the strong coupling constant α_s, of the renormalization and factorization scales, of the PDFs, of Initial and Final State Radiation (ISR and FSR) and two eigentune variations of the A14 tune. Most of these variations have a very small impact on the jet mass distribution, and lead to variations of the best-fit MSR mass of tens of MeV. The jet mass from boosted tops appears to be a robust observable, insensitive to these aspects of Monte Carlo generation.

The main exception is the down variation of the rate of final state radiation, where the central mass value is shifted downwards by 110 MeV. The different mass value is accompanied by a higher value of Ω_{1q}^{∞} = 1.6 GeV and lower value of $x_2 = 0.42$.

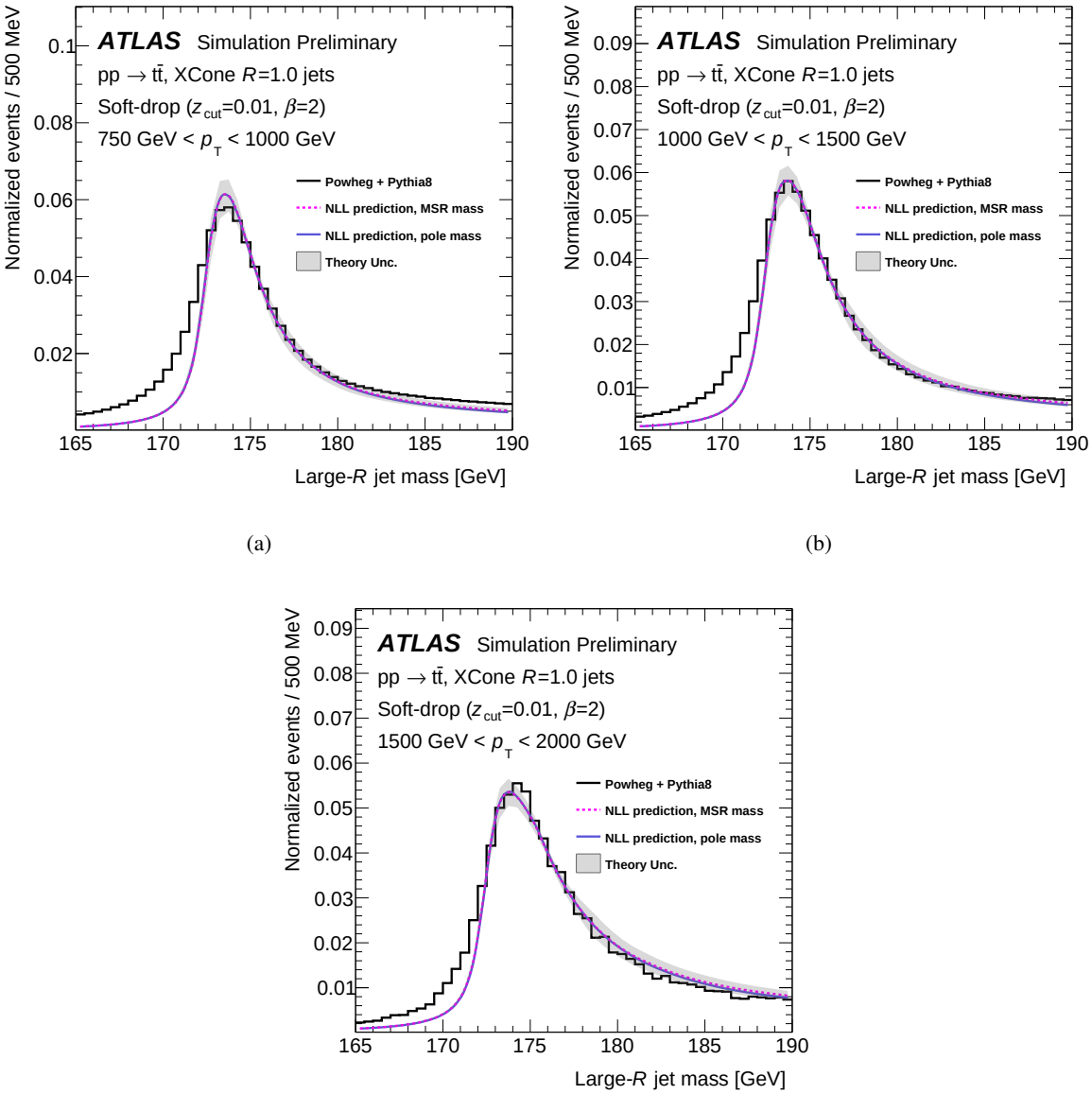

Figure 9: The particle-level jet mass distribution of the nominal POWHEG +PYTHIA 8 sample with MPI=off (black histogram) and the NLL prediction of Ref. [42] which best describe the Monte Carlo prediction (smooth curves). The NLL calculation is performed in the MSR mass scheme (dashed pink curve) and in the pole mass scheme (purple continuous curve). In both mass schemes, the three parameters of the calculation, the top quark mass, Ω_{1q}^{∞} and x_2, are adjusted to find the best description of the three p_{T} intervals used in the calibration procedure. The distributions are normalized and the fit is performed on the interval 172.5 GeV $< m <$ 180 GeV.

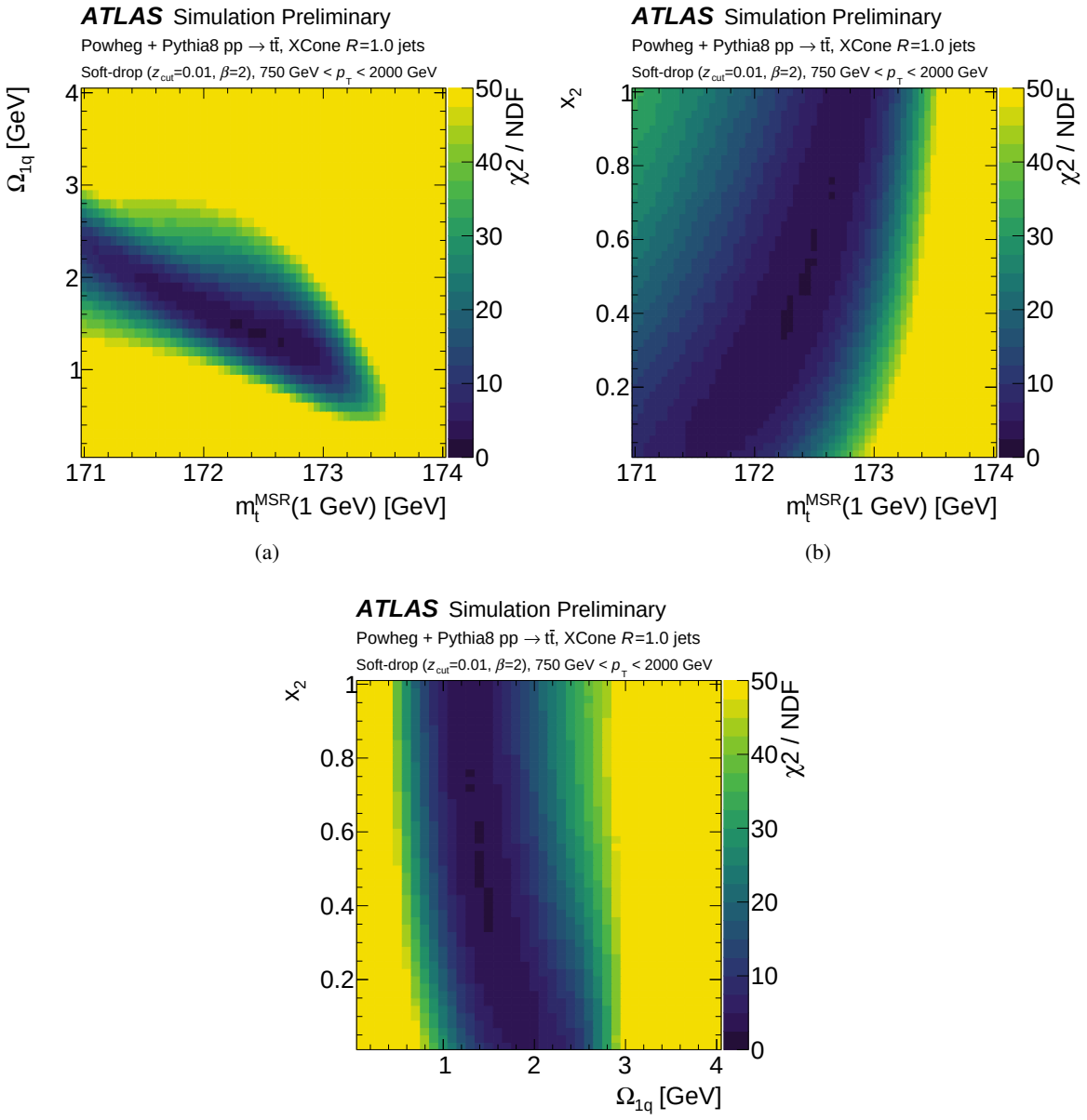

Figure 10: The χ^2 results as a function of the MSR mass $m_t^{\mathrm{MSR}}(1\ \mathrm{GeV})$ and the parameters of the shape function Ω_{1q}^{∞} and x_2, obtained from the fit with the NLL prediction of Ref. [42] to the particle-level jet mass distribution for boosted top quarks in the nominal ATLAS Powheg +Pythia 8 sample. The results are shown in the two-dimensional plane of (a) MSR mass versus Ω_{1q}^{∞}, (b) MSR mass versus x_2 and (c) Ω_{1q}^{∞} versus x_2. In each case, the 2D distribution is obtained by marginalizing over the third parameter. The three parameters of the calculation are adjusted to find the best description of the three p_{T} intervals used in the calibration procedure.

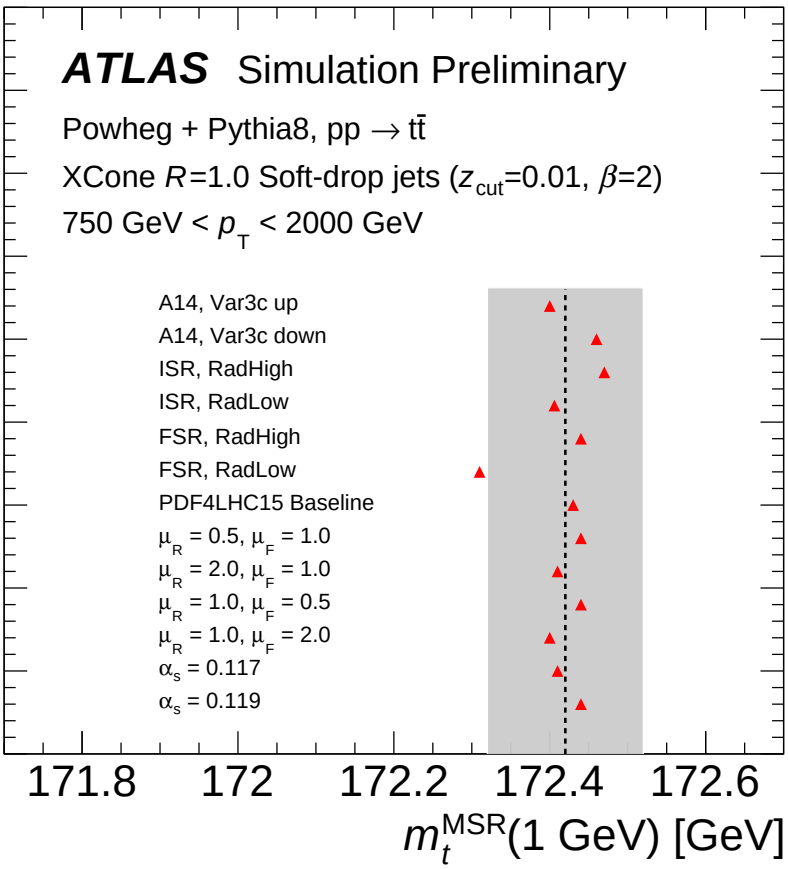

Figure 11: The MSR mass extracted from samples where a given aspect of the $t\bar{t}$ production process is altered with respect to the nominal MC setup (dashed line). The variations affect the PDF, α_s and the renormalization and factorization scale, as well as the rate of initial- and final-state radiation. The vertical band indicates the uncertainty on the nominal fit value.

6.4 Powheg + Herwig 7

The Powheg + Herwig 7 sample is often used to estimate parton shower and hadronization uncertainties for physics analyses of top processes. The predictions for the top jet mass distribution of this sample are compared to Powheg+Pythia 8 in Figure 12. Pythia 8 and Herwig 7 predict very different jet mass distributions; Powheg +Herwig 7 yields a harder jet mass spectrum.

The MSR mass extracted for Powheg + Herwig 7 is:

$$m_t^{MSR}(1\text{ GeV}) = 172.27 \pm 0.09\text{ GeV}, \quad \Omega_{1q}^{\infty} = 1.9 \pm 0.07\text{ GeV}, \quad x_2 = 0.98 \pm 0.12,$$

where the uncertainty is due to the limited Monte Carlo statistics. The two parameters of the shape function absorb the difference between the two jet mass distributions, with significantly higher values for both Ω_{1q}^{∞} and x_2. The mass relation for the Powheg + Herwig 7 setup is, however, compatible within the statistical uncertainty with the nominal result of Eq. 1.

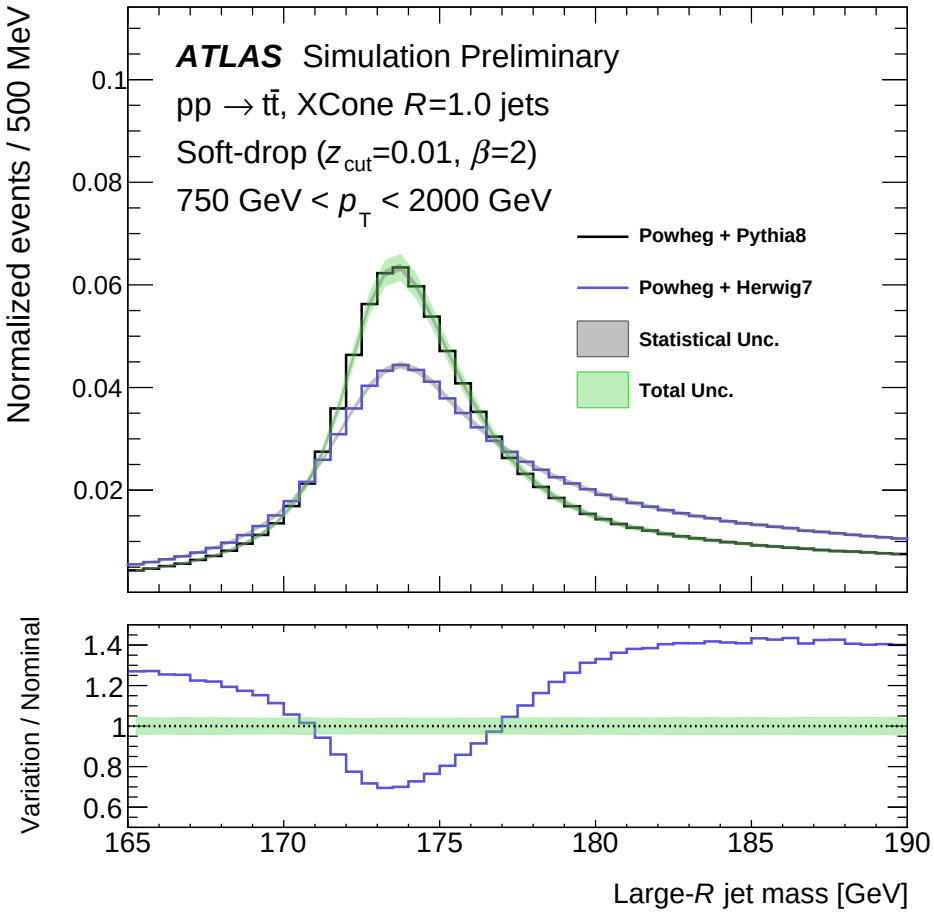

Figure 12: Comparison of $t\bar{t}$ events generated with Powheg and showered with either Pythia 8 or Herwig 7. The total error band accounts for statistical uncertainty, as well as variations of PDFs, α_s and renormalisation / factorisation scales within the nominal Pythia 8 sample. The ratio between nominal and the alternative MC sample is provided in the bottom planel.

6.5 Stability of the result

In this study, the relation between the MSR mass and the MC mass parameter is determined for a specific observable in a limited and extreme kinematic region. Application of this relation as a calibration to precise direct mass measurements corrects for universal effects, *i.e.* effects that lead to the same mass relation for different observables, kinematic regimes and selections. To study whether the relation maintains its validity beyond the environment it was derived in, the stability of the result was investigated by repeating the fit for a number of related observables that are also accessible with the first-principle calculation of Ref. [42].

We vary the user-defined parameters of the soft-drop algorithm to study the effect on the mass relation of the observable used in the fit, within the range of validity of the theory calculation [42]. The analysis is repeated for different sets of grooming parameters which lie in the calculation's region of validity: $\{\beta = 1, z_{\text{cut}} = 0.02\}$, which grooms both soft- and wide-angled radiation more aggressively than the nominal parameters; $\{\beta = 2, z_{\text{cut}} = 0.02\}$, which grooms soft radiation more aggressively but does not alter the soft-drop angular weighting; and $\{\beta = 2, z_{\text{cut}} = 0.005\}$, which is less aggressive.

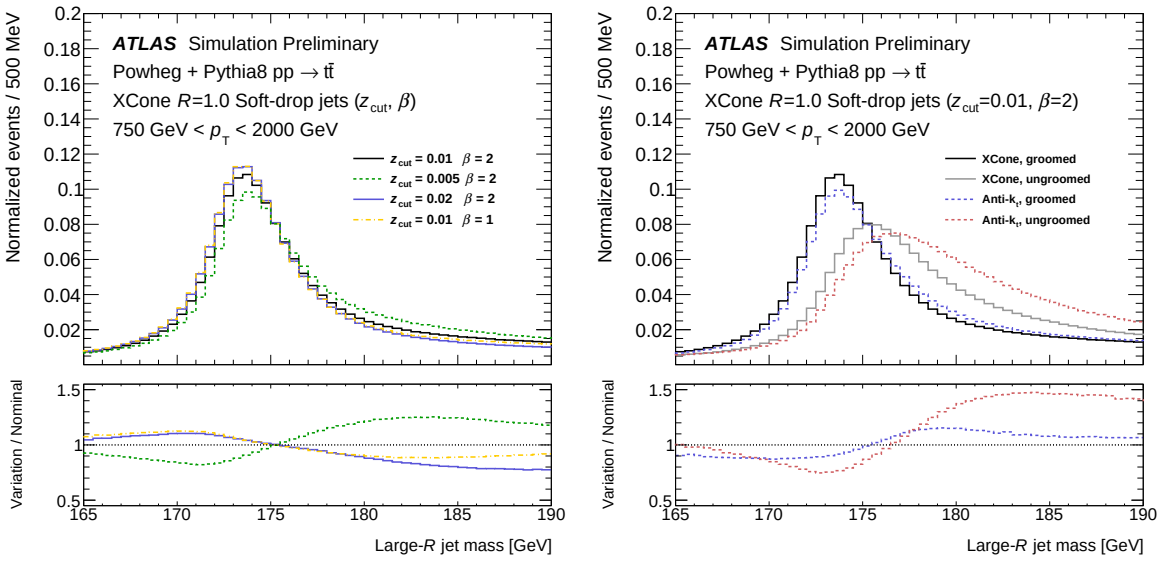

(a) (b)

Figure 13: The impact of different grooming configurations and jet clustering algorithms on the top jet mass distribution for (a) large-R XCone jets groomed with several soft-drop configurations, and (b) ungroomed and groomed (nominal soft-drop configuration) large-R jets clustered with the XCone and anti-k_t algorithms.

Figure 13(a) shows how these variations of the soft-drop configuration shape the jet mass distribution: the least-aggressive grooming option ($\beta = 2$, $z_{\text{cut}} = 0.005$) corresponds to the distribution with the largest mass values, since the fewest components are removed by the grooming procedure. A more aggressive grooming configuration, with larger z_{cut} value reduces pronounced mass tails and shifts the distributions to lower mass values, as do lower values of β.

The fit to the NLL calculation is repeated for each of these distributions. For each comparison, the same grooming parameter settings are used in the Monte Carlo simulation and in the calculation. The fit range is adjusted to follow the average jet mass, to avoid introducing second-order effects due to shifts of the top mass peak. The MSR mass is found to be 172.35 ± 0.05 GeV for $\{\beta = 2, z_{\text{cut}} = 0.005\}$ (less aggressive grooming) and 172.23 ± 0.04 GeV for $\{\beta = 2, z_{\text{cut}} = 0.02\}$ (more aggressive than the nominal). The result for $\{\beta = 1, z_{\text{cut}} = 0.01\}$ (more aggressive for soft and wide-angle radiation) is 172.23 ± 0.04 GeV.

The algorithm used to cluster stable particles into large-R jets also has a non-negligible effect on the jet mass shape, as can be observed in Figure 13(b). The jets clustered with the Anti-k_t and XCone jet reconstruction have different catchment areas and collect different constituents. The difference is clearly observed prior to applying any grooming technique and remains visible with the light grooming applied here. The MSR mass extracted from large-R jets built with the anti-k_t algorithm and the nominal soft-drop grooming parameters is found to be 172.56 ± 0.06 GeV, within 140 MeV of the nominal result.

The maximal variations of the mass relation due to the definition of the mass-sensitive observable are found to be contained within ±200 MeV, within the uncertainties of the procedure. This relation between MC mass and MSR mass is stable at the level of ±200 MeV; this conclusion is compatible with the predictions of the underlying theoretical framework.

7 Conclusions and outlook

In this note, the top quark mass parameter in ATLAS Monte Carlo samples is related to the MSR scheme at a scale of 1 GeV; a short-distance mass scheme that is numerically close to the pole mass [41]. A quantitative relation is determined by comparing Monte Carlo predictions without Underlying Event modelling (MPI=off) for the jet mass distribution of large-R jets containing high-p_{T}, hadronically decaying top quarks to analytical calculations with a first-principles prediction including resummation at next-to-leading-logarithmic accuracy [42].

The relation of the top quark mass parameter in the nominal ATLAS Powheg+Pythia sample to the top quark mass in the MSR mass scheme is found to be $m_t^{\mathrm{MC}} = m_t^{\mathrm{MSR}}(R) + 80$ MeV, for $R = 1$ GeV. The uncertainty of this interpretation of the top quark Monte Carlo mass parameter is approximately $+350/-410$ MeV, with contributions from missing higher orders in the theory predictions ($+230/-310$ MeV), the fit methodology (± 190 MeV) and the underlying event modelling (± 155 MeV).

This study applies the method proposed in Ref. [40] to the ATLAS Monte Carlo samples used in top quark mass measurements. This is a necessary step to translate the central value obtained with a template mass measurement to a well-defined mass scheme. Future advances in the theoretical calculations and the treatment of nonperturbative QCD effects are expected to lead to a considerable improvement in the precision of this calibration procedure, potentially reducing systematic uncertainties on direct top mass measurements to the level required to exploit the high statistics which will be available at the HL-LHC [78].

We have explored the stability of the mass relation by varying aspects of the jet reconstruction algorithm, the soft-drop grooming parameters and the kinematic range. No evidence was found for dependence of the results on the definition of the observable, within the restrictions imposed by the theoretical framework. The compatibility of the results obtained here with those from fits to boosted top quarks produced in e^+e^- collisions yields a further argument for a universal interpretation of the mass relation. However, further effects might come into play in an extrapolation of the mass relation to other observables and a careful assessment must be made of modelling uncertainties in the cailbration of the most precise direct top mass measurements. To take full advantage of the mass relation determined here, a precise template mass measurement based on the jet mass distribution of boosted top quarks [79] is required.

References

[1] ATLAS Collaboration, *The ATLAS Experiment at the CERN Large Hadron Collider*, JINST **3** (2008) S08003 (cit. on p. 2).

[2] ATLAS Collaboration, *Observation of a new particle in the search for the Standard Model Higgs boson with the ATLAS detector at the LHC*, Phys. Lett. B **716** (2012) 1, arXiv: 1207.7214 [hep-ex] (cit. on p. 2).

[3] CMS Collaboration, *CMS Physics Technical Design Report, Volume II: Physics Performance*, J. Phys G **34** (2007) 995 (cit. on p. 2).

[4] CMS Collaboration, *Observation of a new boson at a mass of 125 GeV with the CMS experiment at the LHC*, Phys. Lett. B **716** (2012) 30, arXiv: 1207.7235 [hep-ex] (cit. on p. 2).

[5] L. Evans and P. Bryant, *LHC Machine*, JINST **3** (2008) S08001 (cit. on p. 2).

[6] M. Baak et al., *The global electroweak fit at NNLO and prospects for the LHC and ILC*, Eur. Phys. J. **C74** (2014) 3046, arXiv: 1407.3792 [hep-ph] (cit. on p. 2).

[7] G. Degrassi et al., *Higgs mass and vacuum stability in the Standard Model at NNLO*, JHEP **08** (2012) 098, arXiv: 1205.6497 [hep-ph] (cit. on p. 2).

[8] F. Abe et al., *Observation of top quark production in $\bar{p}p$ collisions*, Phys. Rev. Lett. **74** (1995) 2626, arXiv: hep-ex/9503002 [hep-ex] (cit. on p. 2).

[9] S. Abachi et al., *Observation of the top quark*, Phys. Rev. Lett. **74** (1995) 2632, arXiv: hep-ex/9503003 [hep-ex] (cit. on p. 2).

[10] CMS Collaboration, *Measurement of the top quark mass with lepton+jets final states using pp collisions at $\sqrt{s} = 13$ TeV*, Eur. Phys. J. C **78** (2018) 891, arXiv: 1805.01428 [hep-ex] (cit. on p. 2).

[11] ATLAS Collaboration, *Measurement of the top quark mass in the $t\bar{t} \to$ lepton+jets channel from $\sqrt{s} = 8$ TeV ATLAS data and combination with previous results*, Eur. Phys. J. C **79** (2019) 290, arXiv: 1810.01772 [hep-ex] (cit. on p. 2).

[12] CMS Collaboration, *Combination of the CMS top-quark mass measurements from Run 1 of the LHC*, (2014) (cit. on p. 2).

[13] CDF and D0 Collaborations, *Combination of CDF and D0 results on the mass of the top quark using up 9.7 fb^{-1} at the Tevatron*, (2016), arXiv: 1608.01881 [hep-ex] (cit. on p. 2).

[14] ATLAS, CDF, CMS and D0 Collaborations, *First combination of Tevatron and LHC measurements of the top-quark mass*, (2014), arXiv: 1403.4427 [hep-ex] (cit. on p. 2).

[15] CMS Collaboration, *Measurement of the mass of the top quark in decays with a J/ψ meson in pp collisions at 8 TeV*, JHEP **12** (2016) 123, arXiv: 1608.03560 [hep-ex] (cit. on p. 2).

[16] ATLAS Collaboration, *Measurement of the top quark mass in topologies enhanced with single top quarks produced in the t-channel at $\sqrt{s} = 8$ TeV using the ATLAS experiment*, ATLAS-CONF-2014-055, 2014, URL: https://cds.cern.ch/record/1951323 (cit. on p. 2).

[17] CMS Collaboration, *Measurement of the top quark mass using single top quark events in proton–proton collisions at $\sqrt{s} = 8$ TeV*, Eur. Phys. J. C **77** (2017) 354, arXiv: 1703.02530 [hep-ex] (cit. on p. 2).

[18] CMS Collaboration, *Measurement of the top quark mass in events with a single reconstructed top quark at $\sqrt{s} = 13$ TeV*, (2021) (cit. on p. 2).

[19] CMS Collaboration, *Measurement of the jet mass in highly boosted $t\bar{t}$ events from pp collisions at $\sqrt{s} = 8$ TeV*, Eur. Phys. J. C **77** (2017) 467, arXiv: 1703.06330 [hep-ex] (cit. on p. 2).

[20] A. H. Hoang, *What is the Top Quark Mass?*, Ann. Rev. Nucl. Part. Sci. **70** (2020) 225, arXiv: 2004.12915 [hep-ph] (cit. on pp. 3, 22).

[21] P. Azzi et al., *Report from Working Group 1: Standard Model Physics at the HL-LHC and HE-LHC*, CERN Yellow Rep. Monogr. **7** (2019) 1, ed. by A. Dainese et al., arXiv: 1902.04070 [hep-ph] (cit. on p. 3).

[22] A. Juste et al., *Determination of the top quark mass circa 2013: methods, subtleties, perspectives*, Eur. Phys. J. C **74** (2014) 3119, arXiv: 1310.0799 [hep-ph] (cit. on p. 3).

[23] S. Moch et al., *High precision fundamental constants at the TeV scale*, (2014), arXiv: 1405.4781 [hep-ph] (cit. on p. 3).

[24] J. Bellm et al., *Herwig 7.0/Herwig++ 3.0 release note*, Eur. Phys. J. **C76** (2016) 196, arXiv: 1512.01178 [hep-ph] (cit. on pp. 3, 8).

[25] M. Bahr et al., *Herwig++ Physics and Manual*, Eur. Phys. J. **C58** (2008) 639, arXiv: 0803.0883 [hep-ph] (cit. on p. 3).

[26] A. H. Hoang, S. Plätzer and D. Samitz, *On the Cutoff Dependence of the Quark Mass Parameter in Angular Ordered Parton Showers*, JHEP **10** (2018) 200, arXiv: 1807.06617 [hep-ph] (cit. on p. 3).

[27] S. Argyropoulos and T. Sjöstrand, *Effects of color reconnection on $t\bar{t}$ final states at the LHC*, JHEP **11** (2014) 043, arXiv: 1407.6653 [hep-ph] (cit. on p. 3).

[28] J. R. Christiansen and P. Z. Skands, *String Formation Beyond Leading Colour*, JHEP **08** (2015) 003, arXiv: 1505.01681 [hep-ph] (cit. on p. 3).

[29] G. Corcella, R. Franceschini and D. Kim, *Fragmentation Uncertainties in Hadronic Observables for Top-quark Mass Measurements*, Nucl. Phys. B **929** (2018) 485, arXiv: 1712.05801 [hep-ph] (cit. on p. 3).

[30] H. Brooks and P. Skands, *Coherent showers in decays of colored resonances*, Phys. Rev. D **100** (2019) 076006, arXiv: 1907.08980 [hep-ph] (cit. on pp. 3, 8).

[31] M. Beneke, P. Marquard, P. Nason and M. Steinhauser, *On the ultimate uncertainty of the top quark pole mass*, Phys. Lett. B **775** (2017) 63, arXiv: 1605.03609 [hep-ph] (cit. on p. 3).

[32] A. H. Hoang, C. Lepenik and M. Preisser, *On the Light Massive Flavor Dependence of the Large Order Asymptotic Behavior and the Ambiguity of the Pole Mass*, JHEP **09** (2017) 099, arXiv: 1706.08526 [hep-ph] (cit. on p. 3).

[33] J. Haller et al., *Update of the global electroweak fit and constraints on two-Higgs-doublet models*, Eur. Phys. J. C **78** (2018) 675, arXiv: 1803.01853 [hep-ph] (cit. on p. 3).

[34] U. Langenfeld, S. Moch and P. Uwer, *Measuring the running top-quark mass*, Phys.Rev. **D80** (2009) 054009, arXiv: 0906.5273 (cit. on p. 3).

[35] CMS Collaboration, *Measurement of $t\bar{t}$ normalised multi-differential cross sections in pp collisions at $\sqrt{s} = 13$ TeV, and simultaneous determination of the strong coupling strength, top quark pole mass, and parton distribution functions*, Eur. Phys. J. C **80** (2020) 658, arXiv: 1904.05237 [hep-ex] (cit. on p. 3).

[36] ATLAS Collaboration, *Measurement of lepton differential distributions and the top quark mass in $t\bar{t}$ production in pp collisions at $\sqrt{s} = 8$ TeV with the ATLAS detector*, Eur. Phys. J. C **77** (2017) 804, arXiv: 1709.09407 [hep-ex] (cit. on p. 3).

[37] ATLAS Collaboration, *Measurement of the top-quark mass in $t\bar{t} + 1$-jet events collected with the ATLAS detector in pp collisions at $\sqrt{s} = 8$ TeV*, JHEP **11** (2019) 150, arXiv: 1905.02302 [hep-ex] (cit. on p. 3).

[38] S. Ferrario Ravasio, T. Ježo, P. Nason and C. Oleari, *A theoretical study of top-mass measurements at the LHC using NLO+PS generators of increasing accuracy*, Eur. Phys. J. C **78** (2018) 458, [Addendum: Eur.Phys.J.C 79, 859 (2019)], arXiv: 1906.09166 [hep-ph] (cit. on p. 3).

[39] T. Ježo, J. M. Lindert, P. Nason, C. Oleari and S. Pozzorini, *An NLO+PS generator for $t\bar{t}$ and Wt production and decay including non-resonant and interference effects*, Eur. Phys. J. C **76** (2016) 691, arXiv: 1607.04538 [hep-ph] (cit. on p. 3).

[40] M. Butenschoen et al., *Top Quark Mass Calibration for Monte Carlo Event Generators*, (2016), arXiv: 1608.01318 [hep-ph] (cit. on pp. 3–5, 28).

[41] B. Bachu, A. H. Hoang, V. Mateu, A. Pathak and I. W. Stewart, *Boosted Top Quarks in the Peak Region with N^3LL Resummation*, (2020), arXiv: 2012.12304 [hep-ph] (cit. on pp. 3, 6, 15, 28).

[42] A. H. Hoang, S. Mantry, A. Pathak and I. W. Stewart, *Extracting a Short Distance Top Mass with Light Grooming*, (2017), arXiv: 1708.02586 [hep-ph] (cit. on pp. 3–7, 11, 13, 14, 18, 22–24, 26, 28).

[43] J. Kieseler, K. Lipka and S.-O. Moch, *Calibration of the Top-Quark Monte Carlo Mass*, Phys. Rev. Lett. **116** (2016) 162001, arXiv: 1511.00841 [hep-ph] (cit. on p. 4).

[44] R. Kogler et al., *Jet Substructure at the Large Hadron Collider: Experimental Review*, Rev. Mod. Phys. **91** (2019) 045003, arXiv: 1803.06991 [hep-ex] (cit. on p. 4).

[45] A. J. Larkoski, I. Moult and B. Nachman, *Jet Substructure at the Large Hadron Collider: A Review of Recent Advances in Theory and Machine Learning*, Phys. Rept. **841** (2020) 1, arXiv: 1709.04464 [hep-ph] (cit. on p. 4).

[46] M. Dasgupta, A. Fregoso, S. Marzani and G. P. Salam, *Towards an understanding of jet substructure*, JHEP **09** (2013) 029, arXiv: 1307.0007 [hep-ph] (cit. on p. 4).

[47] A. J. Larkoski, S. Marzani, G. Soyez and J. Thaler, *Soft Drop*, JHEP **05** (2014) 146, arXiv: 1402.2657 [hep-ph] (cit. on p. 4).

[48] M. Dasgupta and G. P. Salam, *Resummation of nonglobal QCD observables*, Phys. Lett. B **512** (2001) 323, arXiv: hep-ph/0104277 (cit. on p. 4).

[49] S. Marzani, L. Schunk and G. Soyez, *A study of jet mass distributions with grooming*, JHEP **07** (2017) 132, arXiv: 1704.02210 [hep-ph] (cit. on p. 4).

[50] S. Marzani, L. Schunk and G. Soyez, *The jet mass distribution after Soft Drop*, Eur. Phys. J. C **78** (2018) 96, arXiv: 1712.05105 [hep-ph] (cit. on p. 4).

[51] C. Frye, A. J. Larkoski, M. D. Schwartz and K. Yan, *Factorization for groomed jet substructure beyond the next-to-leading logarithm*, JHEP **07** (2016) 064, arXiv: 1603.09338 [hep-ph] (cit. on p. 4).

[52] C. Frye, A. J. Larkoski, M. D. Schwartz and K. Yan, *Precision physics with pile-up insensitive observables*, (2016), arXiv: 1603.06375 [hep-ph] (cit. on p. 4).

[53] Z.-B. Kang, K. Lee, X. Liu and F. Ringer, *Soft drop groomed jet angularities at the LHC*, Phys. Lett. B **793** (2019) 41, arXiv: 1811.06983 [hep-ph] (cit. on p. 4).

[54] Z.-B. Kang, K. Lee, X. Liu and F. Ringer,
The groomed and ungroomed jet mass distribution for inclusive jet production at the LHC,
JHEP **10** (2018) 137, arXiv: 1803.03645 [hep-ph] (cit. on p. 4).

[55] Z.-B. Kang, K. Lee, X. Liu, D. Neill and F. Ringer, *The soft drop groomed jet radius at NLL*,
JHEP **02** (2020) 054, arXiv: 1908.01783 [hep-ph] (cit. on p. 4).

[56] ATLAS Collaboration,
Measurement of the Soft-Drop Jet Mass in pp Collisions at $\sqrt{s}$ = 13 TeV with the ATLAS detector,
Phys. Rev. Lett. **121** (2018) 092001, arXiv: 1711.08341 [hep-ex] (cit. on p. 4).

[57] CMS Collaboration, *Measurements of the differential jet cross section as a function of the jet mass in dijet events from proton–proton collisions at $\sqrt{s}$ = 13 TeV*, JHEP **11** (2018) 113,
arXiv: 1807.05974 [hep-ex] (cit. on p. 4).

[58] ATLAS Collaboration,
Measurement of soft-drop jet observables in pp collisions with the ATLAS detector at $\sqrt{s}$ = 13 TeV,
Phys. Rev. D **101** (2020) 052007, arXiv: 1912.09837 [hep-ex] (cit. on p. 4).

[59] J. Mulligan,
Jet substructure measurements in pp *and Pb-Pb collisions at $\sqrt{s_{\mathrm{NN}}}$ = 5.02 TeV with ALICE*, (2020),
arXiv: 2009.07172 [nucl-ex] (cit. on p. 4).

[60] J. Adam et al.,
Measurement of groomed jet substructure observables in p+p collisions at $\sqrt{s}$ =200 GeV with STAR,
Phys. Lett. B **811** (2020) 135846, arXiv: 2003.02114 [hep-ex] (cit. on p. 4).

[61] A. Hoang, S. Mantry, A. Pathak and I. W. Stewart,
Nonperturbative corrections to soft drop jet mass, Journal of High Energy Physics **2019** (2019) 2,
URL: https://doi.org/10.1007/JHEP12(2019)002 (cit. on pp. 4, 5).

[62] S. Fleming, A. H. Hoang, S. Mantry and I. W. Stewart,
Jets from massive unstable particles: Top-mass determination, Phys. Rev. D **77** (7 2008) 074010,
URL: https://link.aps.org/doi/10.1103/PhysRevD.77.074010 (cit. on p. 5).

[63] S. Fleming, A. H. Hoang, S. Mantry and I. W. Stewart,
Top jets in the peak region: Factorization analysis with next-to-leading-log resummation,
Phys. Rev. D **77** (11 2008) 114003,
URL: https://link.aps.org/doi/10.1103/PhysRevD.77.114003 (cit. on p. 5).

[64] A. H. Hoang, A. Jain, I. Scimemi and I. W. Stewart,
Infrared Renormalization Group Flow for Heavy Quark Masses,
Phys. Rev. Lett. **101** (2008) 151602, arXiv: 0803.4214 [hep-ph] (cit. on p. 6).

[65] P. Nason, *A New method for combining NLO QCD with shower Monte Carlo algorithms*,
JHEP **11** (2004) 040, arXiv: hep-ph/0409146 [hep-ph] (cit. on p. 7).

[66] S. Frixione, P. Nason and C. Oleari,
Matching NLO QCD computations with Parton Shower simulations: the POWHEG method,
JHEP **11** (2007) 070, arXiv: 0709.2092 [hep-ph] (cit. on p. 7).

[67] S. Alioli, P. Nason, C. Oleari and E. Re, *A general framework for implementing NLO calculations in shower Monte Carlo programs: the POWHEG BOX*, JHEP **06** (2010) 043,
arXiv: 1002.2581 [hep-ph] (cit. on p. 7).

[68] R. D. Ball et al., *Parton distributions for the LHC Run II*, JHEP **04** (2015) 040,
arXiv: 1410.8849 [hep-ph] (cit. on p. 7).

[69] *Studies on top-quark Monte Carlo modelling for Top2016*, tech. rep. ATL-PHYS-PUB-2016-020, CERN, 2016, URL: https://cds.cern.ch/record/2216168 (cit. on pp. 7, 8).

[70] T. Sjostrand et al., *An Introduction to PYTHIA 8.2*, Comput. Phys. Commun. **191** (2015) 159, arXiv: 1410.3012 [hep-ph] (cit. on p. 7).

[71] *ATLAS Run 1 Pythia8 tunes*, tech. rep. ATL-PHYS-PUB-2014-021, CERN, 2014, URL: https://cds.cern.ch/record/1966419 (cit. on pp. 7, 8, 16, 18, 19).

[72] D. J. Lange, *The EvtGen particle decay simulation package*, Nucl. Instrum. Meth. **A462** (2001) 152 (cit. on p. 7).

[73] ATLAS Collaboration, *Study of top-quark pair modelling and uncertainties using ATLAS measurements at* $\sqrt{s} = 13$ *TeV*, ATL-PHYS-PUB-2020-023, 2020, URL: https://cds.cern.ch/record/2730443 (cit. on p. 8).

[74] J. Alwall et al., *The automated computation of tree-level and next-to-leading order differential cross sections, and their matching to parton shower simulations*, JHEP **07** (2014) 079, arXiv: 1405.0301 [hep-ph] (cit. on p. 8).

[75] I. W. Stewart, F. J. Tackmann, J. Thaler, C. K. Vermilion and T. F. Wilkason, *XCone: N-jettiness as an Exclusive Cone Jet Algorithm*, JHEP **11** (2015) 072, arXiv: 1508.01516 [hep-ph] (cit. on p. 9).

[76] M. Cacciari, G. P. Salam and G. Soyez, *FastJet user manual*, Eur. Phys. J. C **72** (2012) 1896, arXiv: 1111.6097 [hep-ph] (cit. on p. 9).

[77] M. Cacciari, G. P. Salam and G. Soyez, *The Anti-k(t) jet clustering algorithm*, JHEP **0804** (2008) 063, arXiv: 0802.1189 (cit. on p. 9).

[78] A. G. et al., *High-Luminosity Large Hadron Collider (HL-LHC): Technical Design Report V. 0.1*, CERN Yellow Reports: Monographs, Geneva: CERN, 2017, URL: https://cds.cern.ch/record/2284929 (cit. on p. 28).

[79] CMS Collaboration, *Measurement of the jet mass distribution and top quark mass in hadronic decays of boosted top quarks in* pp *collisions at* $\sqrt{s} = 13$ *TeV*, Phys. Rev. Lett. **124** (2020) 202001, arXiv: 1911.03800 [hep-ex] (cit. on p. 28).